

Chemical Technology Division

Waste and Simulant Precipitation Issues

W. F. Steele
C. F. Weber*
D. A. Bostick

*Computational Physics and Engineering Division, ORNL

Prepared for the Tanks Focus Area
DOE Office of Science and Technology

Date Published: January 2001

Prepared by the
OAK RIDGE NATIONAL LABORATORY
Oak Ridge, Tennessee 37831-6285
managed by
UT-BATTELLE, LLC
for the
U.S. DEPARTMENT OF ENERGY
under contract DE-AC05-00OR22725

CONTENTS

LIST OF TABLES	v
1. INTRODUCTION	1
1.1 SCOPE OF WORK	1
1.2 DESCRIPTION OF TASK	1
1.2.1 Savannah River Waste Simulants	1
1.2.2 CST Components	2
1.2.3 Possible Impurity Components	2
1.3 CHEMICAL EQUILIBRIUM MODEL	3
1.4 LABORATORY TESTING PROCEDURES	4
1.4.1 Components Involved in Testing	4
1.4.2 Specific Testing Procedures	6
2. RESULTS	7
2.1 SAVANNAH RIVER SIMULANTS	7
2.1.1 Modeling	7
2.1.2 Laboratory Work	8
2.2 CST COMPONENTS	9
2.2.1 Modeling	9
2.2.2 Laboratory Work	14
2.3 POSSIBLE IMPURITY COMPONENTS	15
2.3.1 Alkaline Earth Elements	15
2.3.2 Metal Oxides and Hydroxides	18
2.3.3 Laboratory Work: Alkaline Earth Elements and Waste Matrix Components	20
3. CONCLUSIONS	21
4. REFERENCES	23
APPENDIX A	A-1
APPENDIX B	B-1

LIST OF TABLES

Table		Page
1	Sequence of chemical addition in the preparation of SRS simulants	3
2	Composition of SRS simulants	5
3	Thermodynamic parameters for titanium species	10
4	Thermodynamic parameters for niobium and zirconium species	13
5	Summary of precipitation testing of CST components in SRS simulants.....	14
6	Comparison of thermodynamic modeling and precipitation testing of CST components in SRS simulants	15
7	Thermodynamic parameters for alkaline earth species	16
8	Thermodynamic parameters for metal oxide and hydroxide species	19
9	Summary of precipitation testing for alkaline earth metals in average SRS simulant.....	20
10	Summary of precipitation testing of waste impurities in SRS simulant	21
11	Comparison of experimental and predicted inventories of impurity materials in average SRS simulant.....	23
A.1	Coefficients for Gibbs energy formation	A-3
A.2	Pitzer parameters in basic model.....	A-5
B.1	Filter 1 – Solids present at point of NaNO ₃ addition in average simulant.....	B-3
B.2	Filter 2 – Solids present at point of NaF addition in average simulant.....	B-4
B.3	Filter 3 – Solids present at point of NaC ₂ O ₄ addition in average simulant.....	B-5
B.4	Filter 4 – Solids present in final solution of average simulant.....	B-6

B.5	Filter 7 – Solids collected after single filtration performed at completion of average simulant preparation	B-7
B.6	Filter 16 – Solids collected after $\text{UO}_2(\text{NO}_3)_2$ added at completion of average simulant preparation	B-8
B.7	Filter 5 – Solids present at point of NaNO_3 addition in high- NO_3^- simulant	B-9
B.8	Filter 8 – Solids present at point of NaF addition in high- NO_3^- simulant.	B-10
B.9	Filter 10 – Solids present at point of $\text{Na}_2\text{C}_2\text{O}_4$ addition in high- NO_3^- simulant	B-11
B.10	Filter 12 – Solids present at point of $\text{Na}_2\text{SiO}_3 \cdot 9\text{H}_2\text{O}$ addition in high- NO_3^- simulant.	B-12
B.11	Filter 6 – Solids present at point of NaNO_3 addition in high- OH^- simulant.	B-13
B.12	Filter 11 – Solids present at point of $\text{Na}_2\text{C}_2\text{O}_4$ addition in high- OH^- simulant.	B-14
B.13	Filter 13 – Solids present in final solution of high- OH^- simulant.....	B-15

1. INTRODUCTION

1.1 SCOPE OF WORK

As Savannah River Site (SRS) personnel have studied methods of preparing high-level waste for vitrification in the Defense Waste Processing Facility (DWPF), questions have arisen with regard to the formation of insoluble waste precipitates at inopportune times. One option for decontamination of the SRS waste streams employs the use of an engineered form of crystalline silicotitanate (CST). Testing of the process during FY 1999 identified problems associated with the formation of precipitates during cesium sorption tests using CST. These precipitates may, under some circumstances, obstruct the pores of the CST particles and, hence, interfere with the sorption process.

In addition, earlier results from the DWPF recycle stream compatibility testing have shown that leaching occurs from the CST when it is stored at 80°C in a high-pH environment. Evidence was established that some level of components of the CST, such as silica, was leached from the CST.

This report describes the results of equilibrium modeling and precipitation studies associated with the overall stability of the waste streams, CST component leaching, and the presence of minor components in the waste streams. The scope of work was requested by SRS¹ and performed according to the ORNL Task Plan (ORNL/CF-99/65).²

1.2 DESCRIPTION OF TASK

The task consists of the activities described in Sects. 1.2.1–1.2.3.

1.2.1 Savannah River Waste Simulants

Modeling and Laboratory Confirmation of the Conditions for Precipitation

Formation. In this task, thermodynamic modeling of simulant waste solutions was performed using the code SOLGASMIX,^{3,4} which solves for chemical equilibrium using

Gibbs energy minimization. Modeling calculations were restricted to the three solutions that have been formulated to represent SRS waste processing operations. The constituent inventories for each type (denoted “average,” “high OH⁻,” or “high NO₃⁻”) ⁵ are listed in Table 1. To confirm the results of the modeling studies, each of the three simulant solutions was prepared according to the chemical sequence delineated in Ref. 5 (see “Solubility of SRS Simulant Components” in Sect. 1.4.1). Any precipitate formed during the addition of the chemicals listed in Table 1 was noted, collected, and subjected to X-ray diffraction (XRD) analysis.

1.2.2 CST Components

Modeling and Laboratory Confirmation of the Conditions for Leaching of Components. In this task, thermodynamic modeling included ions that may be present in solution due to the dissolution of components of the CST manufactured by UOP LLC, its binder, or excess impurities from the manufacturing process. After extensive discussions with all interested parties, modeling was restricted to salts of silicon, titanium, zirconium, and niobium mixed with each simulant and also when mixed with 3 M NaOH. To confirm the results of the modeling, laboratory measurements were undertaken to determine the solubility of each of the above components in each simulant and in 3 M NaOH.

1.2.3 Possible Impurity Components

Modeling and Laboratory Confirmation of the Conditions Under Which Precipitation of Various Metal Oxides, Hydroxides, or Carbonates Will Form in the Simulant Solutions. Here, the alkaline earth elements and a number of others that are expected to be present as trace matrix components were modeled. Magnesium, calcium, strontium, barium, copper, iron, nickel, mercury, lead, and zinc were modeled. To confirm the results of the modeling, laboratory measurements were undertaken to determine the solubility of each of these components in each simulant and 3 M NaOH.

Table 1. Sequence of chemical addition in the preparation of SRS simulants

Chemical component	Manufacturer: Lot no.
Water	Nanopure 18.1 mohm-cm
NaOH	EM Science: 35035515
Al(NO ₃) ₃ ·9H ₂ O	Harrell Industry: 032999
KNO ₃	EM Science: 30242140
CsCl	EM Science: 38317
NaN ₃	J. T. Baker: 007525
NaNO ₂	EM Science: 27062341
Na ₂ CO ₃	EM Science: 3735080822
Na ₂ SO ₄	EM Science: 34162434
NaF	EM Science: 38253850
NaCl	EM Science: 36261648
Na ₂ C ₂ O ₄	EM Science: 38190834
Na ₂ HPO ₄ ·12H ₂ O	J. T. Baker: k33356
Na ₂ SiO ₃ ·9H ₂ O	EM Science: 38093817
Na ₂ MoO ₄ ·2H ₂ O	J. T. Baker: d213361
Final water	

1.3 CHEMICAL EQUILIBRIUM MODEL

The principal computational tool is based on the code SOLGASMIX,^{3,4} which solves for chemical equilibrium using Gibbs energy minimization. Required as input for each species is the Gibbs energy of formation (in practice, the reduced chemical potential μ^0/RT is used), and for aqueous species, parameters to calculate activity coefficients. In this work, the Pitzer model of electrolyte solutions is used for activity coefficients,⁶ which requires the parameters $\beta^{(0)}$, $\beta^{(1)}$, $\beta^{(2)}$, and C for cation-anion interactions. Sometimes, the additional parameters θ and ψ are also needed for interactions involving mixtures. Temperature dependence for each of these parameters is expressed using the functional form

$$F(T) = A + B (T - T_0) + C (1/T_0 - 1/T) + D \ln(T/T_0) + E (T^2 - T_0^2), \quad (1)$$

where $T_0 = 298.15$ K. A represents the parameter value at 25°C, and the other coefficients determine variation with temperature. In practice, some of these are usually zero, as it takes only one or two temperature coefficients to adequately model most

species in the temperature range 25–100°C. Additional coding has been developed to perform nonlinear regression using the basic SOLGASMIX package. Thus, if actual parameter values are not available in the literature (and most are not), then parameter values can be obtained from other data. In this study, a variety of data have been used to determine modeling parameters, including solubilities, activity and osmotic coefficients, vapor pressure measurements, enthalpies, and heat capacities. A more detailed description of the model can be found in Ref. 7.

1.4 LABORATORY TESTING PROCEDURES

1.4.1 Components Involved in Testing

Solubility of SRS Simulant Components. The three types of SRS simulants (denoted “average,” “high OH⁻,” and “high NO₃⁻”) were prepared according to the procedure outlined in Ref. 5. Table 1 presents the sequence of chemical additions used for all SRS simulants, as well as the manufacturer of each chemical. Table 2 lists the final molarities and molalities for each component, as detailed by Walker.⁵ Five hundred milliliters of nanopure water was added to a weighed 1-L volumetric flask. Solid NaOH was added slowly to prevent excessive heating. Once cooled, solid chemical components were then added individually with continuous stirring. The nitrate compounds were added, followed by nitrite, fluoride, chloride, carbonate, sulfate, silicate, phosphate, oxalate, and finally, molybdate salts. If a component did not dissolve completely after at least 24 h of stirring, simulant preparation was stopped momentarily to determine the composition of the solids. The solution temperature and weight were determined at the appearance of solids so that the concentration of dissolved chemical components could be calculated on both a volume and a weight basis. The solution was filtered through a Costar Nuclepore[®] glass-fiber filter having a nominal pore size of 0.7 μm. The filtrate was returned to the 1-L volumetric flask for continued simulant preparation. The filter was air dried and submitted for identification of solids by XRD analysis. Solids collected under this preparation scenario were compared with those obtained from a separate preparation of “average” simulant filtered only at the completion of the addition of all components.

Table 2. Composition of SRS simulants

Primary ion	Concentration (<i>M</i>)			Concentration (<i>m</i>)		
	Average	High OH ⁻	High NO ₃ ⁻	Average	High OH ⁻	High NO ₃ ⁻
Na ⁺	5.600	5.578	5.600	6.343	6.060	6.490
K ⁺	0.015	0.030	0.004	0.017	0.033	0.005
Cs ⁺	0.00014	0.00037	0.00014	0.00016	0.00040	0.00016
OH ⁻	1.918	3.058	1.178	2.172	3.323	1.365
NO ₃ ⁻	2.144	1.080	2.840	2.428	1.174	3.291
NO ₂ ⁻	0.520	0.740	0.370	0.589	0.804	0.429
Al(OH) ₄ ⁻	0.310	0.270	0.320	0.351	0.293	0.371
CO ₃ ²⁻	0.160	0.170	0.160	0.181	0.185	0.185
SO ₄ ²⁻	0.150	0.030	0.220	0.170	0.033	0.255
Cl ⁻	0.025	0.010	0.040	0.028	0.011	0.046
F ⁻	0.032	0.010	0.050	0.036	0.011	0.058
PO ₄ ³⁻	0.010	0.008	0.010	0.011	0.009	0.012
C ₂ O ₄ ²⁻	0.008	0.008	0.008	0.009	0.009	0.009
SiOH ₄ (aq)	0.004	0.004	0.004	0.005	0.004	0.005
MoO ₄ ²⁻	0.0002	0.0002	0.0002	0.0002	0.0002	0.0002

Uranium. The solubility of uranium was determined by adding components of average simulant in the same sequence as previously stated, except that sufficient uranium as uranyl nitrate was added at the end of the preparation for a final total uranium concentration of 1 *mM*. After all the simulant components had been added, the solution was filtered. The uranium content in the final solution was determined by inductively coupled plasma (ICP); identification of the solids was made by XRD analysis.

Components of CST. The solubility of silicate was determined by adding 5.6- to 56-mg increments of Na₂SiO₃·5H₂O to 200 mL of 3 *M* NaOH at 10-min intervals. After 10 min of stirring, the solution was allowed to settle, and the presence of solids was evaluated visually. The solution was filtered at the point when precipitate was first observed; sodium silicate was then added to the filtrate to produce significant quantities of solid. A second filtration was subsequently performed. The second filter was dried for XRD analysis; the filtrate was submitted for ICP analysis. The solubilities of titanium, niobium, and zirconium were similarly determined by adding 1-mL aliquots of 1000-ppm solutions of these elements to 3 *M* NaOH and to each of the SRS simulants.

Alkaline Earth Elements and Waste Matrix Components. Standard (1000-ppm) solutions of magnesium, calcium, strontium, and barium chlorides were added individually to average SRS simulant. A number of elements that are expected to be present as trace matrix components were also tested. These elements were added as the nitrate solutions of Cu(II), Fe(III), Hg(II), Ni(II), Pb(II), and Zn(II). Again, testing procedures involved filtering the simulant after initial observation of precipitate and also after larger quantities of solids were produced for XRD analysis.

1.4.2 Specific Testing Procedures

XRD Analysis of Precipitates. XRD analysis was performed by the Materials and Chemistry Laboratory Incorporated, East Tennessee Technology Park, Oak Ridge, Tennessee. The XRD equipment included a Philips XRG3100 X-ray generator coupled with a VAX3100 computer. Copper radiation was used as the X-ray source. The computer runs standard Philips software for control and analysis of the data generated. The calibration standard is a quartz standard supplied by Philips for use with its instrument. A monthly quality assurance (QA) check of the instrument uses this standard to view response from 20 to 90° 2 θ . Both the intensity and the location of the peaks are documented.

The type of sample preparation used with the supplied filters was dependent on the nature of the specific sample. Samples that consisted of thin films on the filters were attached to a sample holder with a thin coating of petroleum jelly. A small wedge of filter was also attached such that the filter section to be analyzed was at the proper height and position for analysis. Samples that consisted of a thick layer of sample were treated differently. Sample material was removed from the filter, crushed, and packed into a standard XRD holder.

ICP Analysis of Filtrate Solutions. The concentration of dissolved metals in sample filtrates was determined using a Model 61E trace analyzer from Thermo Jarrell Ash. The ICP device is a simultaneous plasma emission spectrometer having a 0.75-m polychromator that is set up to measure 31 elements in the sub-ppm concentration range.

Certified elemental standards are used to standardize the measurement range and correct for interelement interference before each sample run is made. Procedures for instrument calibration and sample treatment followed those presented in EPA Method SW846-6010B.

Mercury Analysis by Cold Vapor Atomic Absorption (CVAA). The solubility of mercury in average simulant was determined, based on EPA Method SW846-7470, using a Model PS2000 automated mercury analyzer from Leeman Laboratories. In this procedure, mercuric ion is initially reduced with stannous chloride to form elemental mercury. An argon sweep gas transfers mercury vapor into an optical cell, where its concentration is determined by the absorbance of a 254-nm mercury emission source versus an optical blank.

2. RESULTS

2.1 SAVANNAH RIVER WASTE SIMULANTS

2.1.1 Modeling

The three types of SRS simulants—denoted “average,” “high OH⁻,” or “high NO₃⁻”—were prepared according to the method described in Ref. 7. In order to apply the equilibrium model to SRS simulants, it is necessary to have reliable estimates of all parameters dealing with the principal ions and their interactions with one another in solution. It is also necessary to have Gibbs energy data for each solid and ionic species. These data have been accumulated through a variety of applications (to wastes at SRS and elsewhere), and are provided in Appendix A. Some of the parameters have been published in the open literature or in government reports. Others have been obtained through rigorous data regression but have not been documented in official publications. A few parameters were evaluated during the course of this study; these fit into the latter category.

The equilibrium model was applied to each of the SRS supernatant simulants at temperatures of 25 and 50°C, and some precipitation was predicted. Cancrinite ($3\text{Al}_2\text{O}_3 \cdot 6\text{SiO}_2 \cdot 3\text{Na}_2\text{O} \cdot 1.68\text{NaNO}_3 \cdot 4.1\text{H}_2\text{O}$) is a sodium aluminosilicate that also includes

a small amount of sodium nitrate. Based on modeling, cancrinite was predicted to form in each of the simulants with little or no silicon remaining in solution at equilibrium. Sodium fluorosulfate, the sodium fluoride–sulfate double salt, was modeled to precipitate only in the high- NO_3^- simulant. In the high- NO_3^- simulant, the maximum calculated concentration of fluoride in solution was on the order of only 0.04 *M*. Gibbsite was predicted to precipitate in both the average and the high- NO_3^- simulants. As expected, gibbsite is more soluble in the high- OH^- solution. The maximum concentration of aluminate in solution at 25°C at which the precipitation of gibbsite did not occur was calculated to be 0.26 *M*. Heating the average simulant to 50°C would ensure complete solubility of the aluminate concentration listed in Table 2 (i.e., >0.30 *M* before precipitation). In the high- NO_3^- simulant, gibbsite precipitated at concentrations above 0.16 *M* in aluminate. In actual waste solutions, the aluminate concentration may be higher due to supersaturation.

For all three simulants, the initial modeling calculations predicted the precipitation of sodium oxalate from solution as the temperature was increased from 25 to 50°C. At 25°C, the calculations predicted complete solubility of oxalate, 0.008 *M*, in each simulant. At 50°C, the model predicted precipitation of all the oxalate present. This may indicate a “quirk” in the present model; the oxalate model will undergo scrutiny and revision in the near future.

2.1.2 Laboratory Work

Solids generated during the preparation of each simulant were either the result of incomplete dissolution of simulant components or of chemical reaction among components. The points at which solids were collected during the preparation of each simulant are summarized in Tables B.1 through B.13 (see Appendix B). Sodium oxalate did not completely dissolve in any of the simulants. Sodium carbonate and nitrate salts were typically found on all filters analyzed, resulting simply from the drying of the saturated simulant solution on the filter media. Similarly, $\text{NaHCO}_3 \cdot 2\text{H}_2\text{O}$ was present on the final filters of the high- OH^- and high- NO_3^- simulants. A tan-colored precipitate was observed in all SRS simulant preparations at the point at which aluminum nitrate was

added to NaOH. Once clarified by filtration, the tan precipitate re-formed and accumulated upon aging of the simulants. XRD analysis indicated the presence of a 7.55-Å phase in the precipitate, which was noted in greater amounts than Al(OH)₃ solids. The compound that had a Bragg angle of 7.55 Å has not yet been identified. Copious amounts of sodium fluorosulfate were formed in the high-NO₃⁻ simulant, as predicted by the thermodynamic model.

Uranium Precipitates. Speciation of the yellow-orange uranium precipitate from average simulant was (UO₂)CO₃·2H₂O, and possibly UO₃·H₂O. The solubility was on the order of 0.03 mM uranium, as determined by ICP. The solubility limit is at least an order of magnitude lower than that observed in sludge sample data provided by SRS staff.

2.2 CST COMPONENTS

2.2.1 Modeling

The three primary components considered here are titanium, niobium, and zirconium. Unlike the constituents of SRS simulants, there are very few data in the literature concerning the solubilities of these elements. While there is adequate qualitative information, even quantitative data at 25°C are somewhat sparse. Although the model predictions are reasonable at 25°C, they are uncertain at higher temperatures.

Titanium. The primary solid in equilibrium with aqueous solutions is TiO₂. As alkalinity increases, hydrolysis of soluble titanium occurs^{8,9} so that in highly alkaline solutions, the dominant ion is Ti(OH)₅⁻. Using an established value¹⁰ for the free energy of TiO₂, the present study sought to estimate that of the ion in order to match available solubility data.

Auger¹¹ measured the solubility of TiO₂ in solutions of concentrated NaOH and KOH at room temperature. His results indicate solubility around 10⁻⁴ M, increasing slightly with hydroxide ion concentration. Ziemniak et al.⁹ measured TiO₂ solubility in solutions of

dilute NaOH and trisodium phosphate (pH <11.8). The latter measurements cover the temperature range 20–280°C and indicate constant solubility (within the error of the data) over the range 20–100°C. Their solubility values are about 10^{-8} M, several orders of magnitude lower than those reported by Auger. It is possible that the solids used were quite different (Ziemniak et al.⁹ fired the TiO₂ at 1400°C) or that equilibrium conditions were not achieved. However, the results of Ziemniak et al.⁹ are consistent with the solubility of natural rutile (TiO₂) in neutral salt solutions.¹² Fraker and Ruff¹³ have noted that corrosion of titanium alloys increases markedly as the pH rises above neutral, indicating that the effect of pH on solubility is dominant.

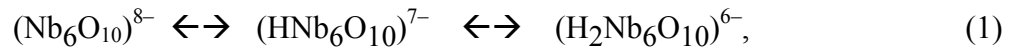
Originally, the model heavily weighted the data of Ziemniak et al.⁹ since it seemed to reflect the latest information, as well as temperature dependence. However, the laboratory experiments at ORNL (see Sect. 2.2.2) indicated solubilities much more consistent with those of Auger.¹¹ Therefore, the revised model considers the data of Auger more strongly. Model parameters were thus selected at 25°C in order to match the data of Auger and the laboratory measurements. Temperature coefficients were selected to maintain constant solubility in the range 25–100°C, consistent with the data of Ziemniak et al.⁹ However, note that this last assumption is uncertain and should be verified by additional experiments. The full set of model parameters for titanium is given in Table 3.

Table 3. Thermodynamic parameters for titanium species

Parameter	Species	Coefficient values	
		A	$C \times 10^{-5}$
μ^0/RT	Ti(OH) ₅ ⁻	-605.3	2.10200
$\beta^{(0)}$	Na ⁺ , Ti(OH) ₅ ⁻	0.1	
$\beta^{(1)}$	Na ⁺ , Ti(OH) ₅ ⁻	1	
θ	NO ₃ ⁻ , Ti(OH) ₅ ⁻	-0.05	

Niobium. Bedford¹⁴ first identified the solid phase hexaniobate (7Na₂O·6Nb₂O₃·32H₂O), which could precipitate from, and be in equilibrium with, aqueous niobate solutions at very high pH. While the exact number of hydration

molecules varies (others¹⁵ use 31), it is verified by Sue.¹⁶ Both Refs. 15 and 16 also mention the formation of another solid at lower pH: $\text{Na}_2\text{O}\cdot\text{Nb}_2\text{O}_5\cdot 7\text{H}_2\text{O}$ (meta-niobate). If calcined with excess NaOH at high temperatures, the hexaniobate forms ortho-niobate, Na_3NbO_4 . This dissolves in water to re-form hexaniobate and excess caustic.¹⁷ Thus, either hexaniobate or meta-niobate will be in equilibrium with alkaline niobate solutions. In solution, the hexaniobate ion is the dominant form, which protonates as the pH is lowered¹⁷:



where the last form is equivalent to $(\text{Nb}_6\text{O}_{18})^{6-}$ and is quickly identified with solid meta-niobate. Stoichiometrically, this ion is the same as NbO_3^- , which is the compound sometimes referred to in the literature.¹⁸ However, this is not the form most likely to exist in solution, because it is possible for polymerization of the hexameric form to occur.¹⁷ The transitions in Eq. (1) occur roughly at pH = 13 and pH = 9 in KOH solutions,¹⁹ although they are not dependent on cation. Additional protonation occurs as the pH is lowered, and at pH = 4.5 the fully protonated solid $\text{H}_6\text{Nb}_6\text{O}_{18}\cdot x\text{H}_2\text{O}$ forms (identical stoichiometrically to Nb_2O_3). Stability constants for the reactions and for the additional protonation $[(\text{H}_2\text{Nb}_6\text{O}_{10})^{6-} \leftrightarrow (\text{H}_3\text{Nb}_6\text{O}_{10})^{5-}]$ have been measured by Etxebarria et al.,²⁰ Spinner,²¹ and Neumann²² in 3 M KCl at 25°C. Solubilities of the potassium and sodium salts in alkaline solutions have been measured by Babko et al.²³ and Sue,¹⁶ respectively. The former work was performed using 1 M KNO_3 , although the authors claim no effects of ionic strength and no temperature dependence in the range 17–25°C. Results at 20°C are available for both cases.

The model includes the four aqueous species, utilizing the HSC database¹⁰ for the Gibbs energies of the 6⁻-species (temperature dependent) and the equilibrium constants of Spinner²¹ to obtain Gibbs energies for the other species at 25°C. The Gibbs energies of the 7⁻- and 5⁻-species are estimated at 18°C using the titration data of Sue¹⁶ and by assuming that the 8⁻-species must be dominant at pH = 14 but not at pH = 12. The

estimates at two temperatures allow for a single temperature coefficient to be calculated for each ion. Extrapolations far from the range 18–25°C should be done cautiously.

The solid, $\text{Na}_2\text{O}\cdot\text{Nb}_2\text{O}_5\cdot 7\text{H}_2\text{O}$, was evaluated as a part of the titration at 18°C and a Gibbs energy was determined for the hydrated salt.¹⁶ Sue¹⁶ also stated a solubility in pure water for each of the salts at 20°C, which were then used to obtain a Gibbs energy. The $\text{Na}_2\text{O}\cdot\text{Nb}_2\text{O}_5\cdot 7\text{H}_2\text{O}$ can be dehydrated by moderate heating, and the resulting anhydrous salt has very different solubility properties.²⁴ While the latter form might exist in the original CST structure, once solubilization occurs, only the hydrated solid is of interest.

Stability constants are available at various ionic strengths in KCl media. In general, we assume that speciation is independent of the salt solution, so these results will be applied to the NaNO_3 – NaOH solutions encountered in waste processing. Regression of the stability constants allows a determination of Pitzer parameters for interactions between sodium and each of the niobate aqueous species, with results shown in Table 4.

As a result of laboratory (ORNL) experiments, minor adjustments were made in the Gibbs energy of the salt $7\text{Na}_2\text{O}\cdot 6\text{Nb}_2\text{O}_3\cdot 32\text{H}_2\text{O}$. In addition, temperature dependence of this solid was included in the calculations, so that solubility at 50°C is about 1.5 times that at 25°C. No quantitative data are available to justify this point, although Smith and Van Haagen¹⁵ noted: “It is difficultly soluble even in hot water.” Also, a Pitzer mixing parameter, θ , was added, as noted in Table 4.

Zirconium. This element is quite similar to titanium, as it is directly below it in the periodic table. Thus, the solid phase in equilibrium with aqueous solution is ZrO_2 , and the principal ion complex in highly alkaline solutions⁸ is $\text{Zr}(\text{OH})_5^-$. The Gibbs energy for the solid was obtained from the HSC database,¹⁰ and the value for the ion was obtained as a part of this study. In addition, Pitzer parameters for interaction of Na^+ with the zirconate ion were also derived in this work.

While numerous studies have been made of zirconium ion hydrolysis and solubility in neutral and acidic solutions, few have been performed using alkaline solutions. The

solubility data of Sheka and Pevzner²⁵ in NaOH solutions at 25°C forms the foundation for this analysis. Regression of these data was used to determine the Gibbs energy of the zirconate ion and Pitzer parameters for its interaction with sodium. Data of Bilinski et al.²⁶ in neutral solutions show constant solubility between 20 and 40°C, and this is used to justify an assumption that solubility is constant in alkaline solutions as well. The predictions of Slobodov et al.²⁷ above 100°C are also consistent with this assumption. Imposing such constancy on the temperature range 25–100°C allows calculation of temperature coefficients for the Gibbs energy and Pitzer parameters, which are given in Table 4.

Table 4. Thermodynamic parameters for niobium and zirconium species

Parameter	Species	Coefficient values	
		A	$C \times 10^{-5}$
μ^0/RT	Hexaniobate	-9258.2	28.52500
μ^0/RT	meta-Niobiate	-9950.27	33.55915
μ^0/RT	Nb(aq) ⁸⁻	-2342.54	7.00180
μ^0/RT	Nb(aq) ⁷⁻	-2369.94	7.57212
μ^0/RT	Nb(aq) ⁶⁻	-2395.27	8.09770
μ^0/RT	Nb(aq) ⁵⁻	-2418.29	8.45829
$\beta^{(0)}$	Na ⁺ , Nb(aq) ⁸⁻	0.5	
$\beta^{(1)}$	Na ⁺ , Nb(aq) ⁸⁻	60	
C	Na ⁺ , Nb(aq) ⁸⁻	-0.1	
$\beta^{(0)}$	Na ⁺ , Nb(aq) ⁷⁻	0.9542	
$\beta^{(1)}$	Na ⁺ , Nb(aq) ⁷⁻	46.3351	
C	Na ⁺ , Nb(aq) ⁷⁻	-0.1871	
$\beta^{(0)}$	Na ⁺ , Nb(aq) ⁶⁻	1.5768	
$\beta^{(1)}$	Na ⁺ , Nb(aq) ⁶⁻	32.1812	
C	Na ⁺ , Nb(aq) ⁶⁻	-0.327	
$\beta^{(0)}$	Na ⁺ , Nb(aq) ⁵⁻	1.9895	
$\beta^{(1)}$	Na ⁺ , Nb(aq) ⁵⁻	19.7627	
C	Na ⁺ , Nb(aq) ⁵⁻	-0.4402	
θ	NO ₃ ⁻ , Nb(aq) ⁸⁻	0.7	
μ^0/RT	Zr(OH) ₅ ⁻	-666.262	2.28913
μ^0/RT	ZrO ₂	-419.444	1.31989
$\beta^{(0)}$	Na ⁺ , Zr(OH) ₅ ⁻	0.0387	-9.69E-05
$\beta^{(1)}$	Na ⁺ , Zr(OH) ₅ ⁻	1.3382	-1.30E-03
θ	NO ₃ , Zr(OH) ₅ ⁻	0.5	

Results of the ORNL solubility measurement experiments (see Sect. 2.2.2) indicated that the original model was fairly accurate in its solubility prediction. However, there was some indication of a “salting-out” effect (i.e., a decrease in solubility with the increase of anions other than hydroxide). This is in contrast to zirconium behavior in neutral and acidic solutions, where no effect of ionic strength is observed.²⁸ An improved estimate of the solubility in the three SRS simulants was obtained by adding the Pitzer mixture parameter, θ , for interactions between nitrate and zirconate ions.

2.2.2 Laboratory Work

A comparison of the concentrations at which precipitation of a CST component was first visually observed and the solubility as determined by ICP indicates that solutions of these components in SRS simulants are initially supersaturated. With longer mixing times (>150 h), precipitate formation was often observed. Therefore, thermodynamic modeling of CST components as well as the remaining elements tested used solubility data based on ICP analysis of aged solutions (Table 5). Silicate is soluble up to $1 \times 10^{-2} M$; titanium and niobium have solubility limits on the order of $1 \times 10^{-3} M$ in SRS simulants. Zirconium is least soluble in high- NO_3^- simulant and is present only at levels of $3 \times 10^{-5} M$ and $7 \times 10^{-5} M$ in average and high- OH^- simulants, respectively. Because crystalline solids were formed in the presence of only niobium, the chemical composition of the remaining CST components could not successfully be identified by XRD analysis. Niobium formed a sodium oxide precipitate in all SRS simulants. Table 6 compares the results of the modeling with the laboratory solubility measurements for the CST components.

Table 5. Summary of precipitation testing of CST components in SRS simulants

SRS simulant	SiO_3^{2-}		Ti(IV)		Niobium		Zirconium	
	ppm	M	ppm	M	ppm	M	ppm	M
Average	NA	NA	$18. \pm 1.$	$3.74\text{E-}04$	12.0 ± 0.2	$1.29\text{E-}04$	6.1 ± 0.6	$2.65\text{E-}05$
High OH^-	NA	NA	15.2 ± 0.4	$3.17\text{E-}04$	6.8 ± 0.5	$7.30\text{E-}05$	17.0 ± 0.6	$7.35\text{E-}05$
High NO_3^-	NA	NA	14.1 ± 0.2	$2.94\text{E-}04$	10.9 ± 0.9	$1.17\text{E-}04$	2.0 ± 0.3	$8.43\text{E-}06$
3 M NaOH	850 ± 40	$1.12\text{E-}02$	7.1 ± 0.3	$1.49\text{E-}04$	3.2 ± 0.1	$3.44\text{E-}05$	NA	NA

Note: NA = Not analyzed.

Table 6. Comparison of thermodynamic modeling and precipitation testing of CST components in SRS simulants

Simulant	Titanium ($10^4 M$)		Niobium ($10^4 M$)		Zirconium ($10^5 M$)	
	Expt.	Calc.	Expt.	Calc.	Expt.	Calc.
Average	3.74	1.46	1.29	1.26	2.65	2.2
High NO_3^-	3.17	2.21	0.73	0.63	7.35	13
High OH^-	2.94	1.01	1.17	1.18	0.843	0.6

Note: Expt. = experimental; Calc. = calculated.

2.3 POSSIBLE IMPURITY COMPONENTS

2.3.1 Alkaline Earth Elements

The focus of this section is the behavior of elements Mg, Ca, Sr, and Ba. In solution, each is represented as the ion of 2+ charge. Although minor hydrolysis occurs, the solubilities of these elements are so low that ion complexes are inconsequential in the overall modeling task. All form solid hydroxides that are highly insoluble except for $\text{Ba}(\text{OH})_2$. Solids formed with sulfate or carbonate are also highly insoluble, but the nitrate and chloride salts are quite soluble. Thermodynamic data are much more plentiful for these elements than for the CST components. In fact, most of the activity coefficient parameters are available at 25°C, and some are available through the range 0–100°C; the values used are given in Table 7. Gibbs energies for each aqueous ion were obtained from the HSC database,¹⁰ and those for solids, from equilibrium constants or regression of solubility data. In the original model, only hydroxide solids were considered. However, the solubility studies (see the following discussion) indicated carbonates and BaSO_4 as well.

Magnesium. Activity coefficient parameters for magnesium-chloride interactions were obtained from Ref. 6, and those for magnesium-nitrate interactions were regressed from solubility data. The Gibbs energy for $\text{Mg}(\text{OH})_2$ was obtained from Gibbs energies of Mg^{2+} and OH^- , and the equilibrium constant expression, from McGee and Hostetler.²⁹

Table 7. Thermodynamic parameters for alkaline earth species

Parameter	Species	Coefficient values ^a				
		A	B	C	D	E
μ^0/RT	Mg ²⁺	-183.152		56058.800		
μ^0/RT	Ca ²⁺	-223.023		65385.050		
μ^0/RT	Sr ²⁺	-227.41		66231.880		
μ^0/RT	Ba ²⁺	-226.249		64775.420		
μ^0/RT	Mg(OH) ₂	-335.103		111577.800		
μ^0/RT	Ca(OH) ₂	-361.484		100593.300	43.38678	
μ^0/RT	Sr(OH) ₂ ·8H ₂ O	-1128.28		403729.200		
μ^0/RT	Ba(OH) ₂ ·8H ₂ O	-1125.12		398805.500		5.05E-05
μ^0/RT	CaCO ₃	-455.4	-0.06766	152264.900		
μ^0/RT	SrCO ₃	-461.632		152934.400		-9.17E-05
μ^0/RT	BaCO ₃	-458.846		164567.800	-58.2767	
μ^0/RT	BaSO ₄	-549.53		176495.900		
$\beta^{(0)}$	Mg ²⁺ , NO ₃ ⁻	-0.0071		1.02E+03	-1.352	
$\beta^{(1)}$	Mg ²⁺ , NO ₃ ⁻	-3.2092		3.67E+05	-1078	
C	Mg ²⁺ , NO ₃ ⁻	0.0204		-3.18E+01	-0.02244	
$\beta^{(0)}$	Mg ²⁺ , Cl ⁻	0.3512	-9.32E-04			5.94E-07
$\beta^{(1)}$	Mg ²⁺ , Cl ⁻	1.6512	-0.01094			2.60E-05
C	Mg ²⁺ , Cl ⁻	0.0023	-8.84E-05			8.55E-08
$\beta^{(0)}$	Ca ²⁺ , NO ₃ ⁻	0.1581		457.6	-1.1412	
$\beta^{(1)}$	Ca ²⁺ , NO ₃ ⁻	1.9546		-3.33E+03	12.49	
C	Ca ²⁺ , NO ₃ ⁻	-0.0019		-1.84E+01	0.04292	
$\beta^{(0)}$	Ca ²⁺ , Cl ⁻	0.3051		128.4	-0.3924	
$\beta^{(1)}$	Ca ²⁺ , Cl ⁻	1.7149		-3192	11.52	
C	Ca ²⁺ , Cl ⁻	0.0009		-6.366	0.00327	
$\beta^{(0)}$	Sr ²⁺ , NO ₃ ⁻	0.1018		74.88		
$\beta^{(1)}$	Sr ²⁺ , NO ₃ ⁻	1.6496		3.40E+03		
C	Sr ²⁺ , NO ₃ ⁻	-0.0025		-2.49E+00		
$\beta^{(0)}$	Sr ²⁺ , Cl ⁻	0.2858				
$\beta^{(1)}$	Sr ²⁺ , Cl ⁻	1.6673				
C	Sr ²⁺ , Cl ⁻	-0.0005				
$\beta^{(0)}$	Sr ²⁺ , OH ⁻	0.0782		1.309		
$\beta^{(1)}$	Sr ²⁺ , OH ⁻	1.3092		-392.6		
$\beta^{(0)}$	Ba ²⁺ , NO ₃ ⁻	1.0173		-1479		
$\beta^{(1)}$	Ba ²⁺ , NO ₃ ⁻	-4.617		4.54E+03		
C	Ba ²⁺ , NO ₃ ⁻	-0.081		5.92E+01		
$\beta^{(0)}$	Ba ²⁺ , Cl ⁻	0.2628				
$\beta^{(1)}$	Ba ²⁺ , Cl ⁻	1.4963				
C	Ba ²⁺ , Cl ⁻	-0.0069				
$\beta^{(0)}$	Ba ²⁺ , OH ⁻	0.1455		-94.04		
$\beta^{(1)}$	Ba ²⁺ , OH ⁻	-0.3718		956.8		
C	Ba ²⁺ , OH ⁻	-0.0049				

^a From Eq (1).

The resulting solubility predictions are consistent with the estimates of Phillips et al.³⁰ and are sufficiently low that no other analysis was required.

Calcium. Several activity coefficient parameters were taken from past ORNL studies.³¹ Pitzer parameters for calcium-chloride interactions were obtained from Pitzer,⁶ and those for calcium-nitrate interactions were regressed from solubility data. The solubility data of Yeatts and Marshall³² for Ca(OH)_2 in NaNO_3 solutions were used to estimate the Gibbs energy of Ca(OH)_2 simultaneously with the Pitzer parameters for Ca-OH interactions. These authors also provide data for $\text{CaCO}_3 + \text{Ca(OH)}_2$ solubility in NaNO_3 solutions. However, these data were not useful due to the much lower solubility of CaCO_3 . The Gibbs energy of CaCO_3 was therefore obtained from the equilibrium constant expression of Plummer and Busenberg.³³

Strontium. Pitzer parameters for the interaction Sr- NO_3 were regressed from solubility data. The Gibbs energy of Sr(OH)_2 was obtained by regressing solubility data in pure water and salt solutions.³⁴ Also a result of this regression were Pitzer parameters for Sr^{2+} -OH⁻ ion interactions. The Gibbs energy of SrCO_3 was obtained using the equilibrium constant of Plummer and Busenberg.³⁵

Barium. Activity coefficient parameters for barium-nitrate interactions were obtained by regressing solubility data of $\text{Ba(NO}_3)_2$ in pure water and in NaNO_3 solutions.

Solubilities of Ba(OH)_2 in water and in NaOH solutions³⁴ were used to obtain the Gibbs energy for this solid and the Pitzer parameters for Ba-OH ion interaction. In a manner similar to that used for models for calcium and strontium, BaCO_3 was modeled using the equilibrium constant of Busenberg and Plummer.³⁶ Finally, the Gibbs energy of BaSO_4 was obtained by regressing solubility data.³⁴ When Pitzer parameters were assumed to be zero for barium-sulfate interactions, good results were obtained. Therefore, no other action was taken.

2.3.2 Metal Oxides and Hydroxides

A number of transition metals are expected to be present as impurities in the CST material or the SRS waste. The solids in equilibrium with aqueous solutions are common oxides and hydroxides with low solubilities. All of the elements considered undergo significant hydrolysis, and, in alkaline solutions, most of them will appear as anionic or neutral complexes.⁸ For our purposes, a single complex was chosen for each element and Gibbs energies were adapted from those in the HSC database¹⁰ (which usually had different hydrations). Solubility data (most obtained from the compendium by Linke³⁴) are plentiful in comparison with those for the CST components, and most of the predictions are reliable in the range 20–70°C. Results are given in Table 8.

Copper. The principal ionic complex is $\text{Cu}(\text{OH})_4^{2-}$. This complex is the only one considered, even though others may be significant for $\text{pH} < 13$. The principal solid is $\text{Cu}(\text{OH})_2$, although CuO or some other hydrate may be the actual solid. Solubility data at 25, 50, and 75°C in NaOH solutions were regressed to obtain Gibbs energy for the solid and Pitzer parameters for the interaction between sodium and the copper anion complex.

Iron(II). The ion complex is $\text{Fe}(\text{OH})_3^-$, and the principal solid is $\text{Fe}(\text{OH})_2$. At 25°C, solubility data in NaOH solutions³⁴ were used to obtain the Gibbs energy and Pitzer parameters of the solid. Temperature coefficients were obtained from data in KOH solutions at 40 and 60°C (assuming that the behavior in NaOH would be identical) and dilute NaOH/ Na_3PO_4 solutions between 25 and 80°C.

Iron(III). In a manner similar to that for Fe(II), the ion complex for Fe(III) is $\text{Fe}(\text{OH})_4^-$. However, the preferred solid phase is Fe_2O_3 , because various hydrations seem to be less stable. Solubility data in NaOH solutions³⁷ are available at 30, 50, 60, and 76°C and were regressed to obtain the parameters listed in Table 8.

Mercury. This element is the only metal considered for which the ion complex is not anionic; rather, the preferred species is the neutral complex, $\text{Hg}(\text{OH})_2^0$. Solid HgO

Table 8. Thermodynamic parameters for metal oxide and hydroxide species

Parameter	Species	Coefficient values ^a	
		A	C
μ^0/RT	$\text{Cu}(\text{OH})_4^{2-}$	-264.62	109444.000
μ^0/RT	$\text{Fe}(\text{OH})_3^-$	-256.62	97588.100
μ^0/RT	$\text{Fe}(\text{OH})_4^-$	-347.628	124975.700
μ^0/RT	$\text{Zn}(\text{OH})_4^{2-}$	-348.744	135462.300
μ^0/RT	$\text{Pb}(\text{OH})_3^-$	-232.318	87548.170
μ^0/RT	$\text{Hg}(\text{OH})_2$	-108.728	22736.440
μ^0/RT	$\text{Cu}(\text{OH})_2$	-146.322	57712.000
μ^0/RT	$\text{Fe}(\text{OH})_2$	-204.74	68199.200
μ^0/RT	Fe_2O_3	-309.858	92148.210
μ^0/RT	$\text{Zn}(\text{OH})_2$	-224.627	73332.790
μ^0/RT	PbO	-75.054	25369.240
μ^0/RT	HgO	-21.303	8397.590
$\beta^{(0)}$	$\text{Na}^+, \text{Cu}(\text{OH})_4^{2-}$	0.303	-5.42E+01
$\beta^{(1)}$	$\text{Na}^+, \text{Cu}(\text{OH})_4^{2-}$	3.1816	5.00E+03
$\beta^{(0)}$	$\text{Na}^+, \text{Fe}(\text{OH})_3^-$	0.1111	-2.38E+02
$\beta^{(1)}$	$\text{Na}^+, \text{Fe}(\text{OH})_3^-$	-0.6271	-3.48E+03
$\beta^{(0)}$	$\text{Na}^+, \text{Fe}(\text{OH})_4^-$	0.0649	-1.15E+02
$\beta^{(1)}$	$\text{Na}^+, \text{Fe}(\text{OH})_4^-$	-3.865	
$\beta^{(0)}$	$\text{Na}^+, \text{Zn}(\text{OH})_4^{2-}$	0.1522	1.82E+02
$\beta^{(1)}$	$\text{Na}^+, \text{Zn}(\text{OH})_4^{2-}$	3.3788	-1.16E+04
$\beta^{(0)}$	$\text{Na}^+, \text{Pb}(\text{OH})_3^-$	0.157	-1.62E+02
$\beta^{(1)}$	$\text{Na}^+, \text{Pb}(\text{OH})_3^-$	0.6186	2.31E+02
λ	$\text{Na}^+, \text{Hg}(\text{OH})_2^0$	0	
λ	$\text{NO}_3^-, \text{Hg}(\text{OH})_2^0$	-0.0973	
λ	$\text{OH}^-, \text{Hg}(\text{OH})_2^0$	-0.0403	

^aFrom Eq. (1).

occurs in two forms (red and yellow). The behaviors of these two forms are quite similar—probably within the error of the data. The data for yellow HgO were used because they were somewhat more amenable to our analysis. By using solubility data in NaOH + NaNO₃ solutions at 25°C, the ion-neutral Pitzer parameter, λ was obtained, as well as the Gibbs energy of the solid. Temperature coefficients for the latter were obtained from regression of solubility data at higher temperatures in water alone. The assumption of a constant value of λ probably creates no appreciable error.

Lead. The primary ion complex is $\text{Pb}(\text{OH})_3^-$, and the primary solid is PbO. Solubility data at 18 and 60°C in NaOH solutions were used to obtain the Pitzer parameters and Gibbs energy of the solid, as listed in Table 8.

Zinc. The primary ion complex is $\text{Zn}(\text{OH})_4^{2-}$, and the primary solid is $\text{Zn}(\text{OH})_2$. Solubility data at 25–75°C in NaOH solutions were regressed to obtain all parameters. Recalculations are quite good for NaOH >0.3 *m* but deviate below this threshold, probably because other ion complexes become important as pH is decreased.

2.3.3 Laboratory Work: Alkaline Earth Elements and Waste Matrix Components

Table 9 summarizes the solubility limits of common alkaline earth elements in average SRS simulant. Calcium, strontium, and barium are soluble at the level of a few parts per million. Magnesium could not be observed below the detection limit of the ICP technique, indicating that its solubility is less than $2 \times 10^{-5} M$. Again, the chemical forms of the calcium and barium precipitates could not be determined by XRD, owing to their amorphous structures. Strontium was found to be present as carbonate, whereas barium was present as the sulfate salt.

For the metal oxides and hydroxides, the results of the solubility tests are reported in Table 10. Lead is the most soluble of the transition metals studied ($1 \times 10^{-1} M$), followed closely by copper ($3.49\text{E}-03 M$). Nickel is the least soluble, with a solubility limit that is less than $1 \times 10^{-5} M$.

Table 9. Summary of precipitation testing for alkaline earth metals in average SRS simulant

Element	Solubility limit	
	ppm	<i>M</i>
Sr ²⁺	2.7 ± 0.2	3.1E-05±7%
Ba ²⁺	2.1 ± 0.1	1.7E-05±5%
Ca ²⁺	1.1 ± 0.1	2.7E-05±9%
Mg ²⁺	<0.6 ± 0.4	<2.3E-05

Table 10. Summary of precipitation testing of waste impurities in SRS simulant

Impurity	Solubility limit	
	ppm	<i>M</i>
Cu(II)	222 ± 3	3.49E-03
Fe(III)	8.8 ± 0.7	1.57E-04
Hg(II)	100 ± 10	5.11E-04
Ni(II)	<0.80 ± 0.03	<1.36E-05
Pb(II)	21,200 ± 900	1.03E-01
Zn(II)	3,069 ± 18	4.69E-02

3. CONCLUSIONS

The thermodynamic modeling of the simulant solutions showed the possibility of metastable solutions. Cancrinite was predicted to form in each of the simulants with little or no silicon remaining in solution at equilibrium. Sodium fluorosulfate, the sodium fluoride–sulfate double salt, was predicted to precipitate only in the high-NO₃⁻ simulant. In the high-NO₃⁻ simulant, the maximum calculated concentration of fluoride in solution was on the order of only 0.04 *M*. Gibbsite was predicted to precipitate in both the average- and the high-NO₃⁻ simulants. As expected, gibbsite is more soluble in the high-OH⁻ solution. The maximum concentration of aluminate in solution at 25°C at which the precipitation of gibbsite did not occur was calculated to be 0.26 *M*. Heating the average simulant to 50°C would ensure complete solubility of the aluminate concentration listed in Table 2 (i.e., >0.30 *M* before precipitation). In the high-NO₃⁻ simulant, gibbsite precipitated at concentrations above 0.16 *M* in aluminate.

For all three simulants, the initial modeling calculations predicted the precipitation of sodium oxalate from solution as the temperature was increased from 25 to 50°C. At 25°C, the calculations predicted complete solubility of oxalate, 0.008 *M*, in each simulant. At 50°C, the model predicted precipitation of all the oxalate present. Results of the laboratory solubility studies (contained in Appendix B) were in contrast to the calculations at 25°C, indicating the necessity of carrying out a reassessment of the solubility data on oxalates in the simulant solutions.

In addition, some recent research on the solubility of cancrinite in highly alkaline solutions raises a question about the accuracy of its ppm solubility therein. Recent measurements from the Ian Wark Research Institute, University of South Australia, which feature the work of Andrea Gerson and Jonas Addai-Mensah,³⁸⁻⁴⁰ substantiate the finding of low solubility of cancrinite in NaOH solutions. However, the concentration appears to be several orders of magnitude higher than the ppm levels derived in the calculations of the present research. The literature notes the difficulties in obtaining “equilibrium” solutions and discusses the effects of supersaturation and metastability. It covers a temperature range of 90 to 160°C, hydroxide concentrations up to 5.4 *M*, and Al(OH)₃ concentrations up to 2.2 *M*. Extrapolation (roughly, by eyeball) seems to point to a solubility limit somewhat less than 10⁻³ *M* for, say, the average simulant at 25°C. The process appears to be under kinetic control and therefore very dependent on the specific experimental conditions. A review of the recent work and an update of the model to reflect those results are recommended.

In Tables 6 and 11, solubilities calculated by the thermodynamic model are compared with results obtained in the laboratory studies. Since all the experiments were performed at room temperature (25–30°C), it is not possible to evaluate model predictions at higher temperatures. As seen in Table 6, the predictions of CST components are reasonably close to the experimental values. However, the experimental results for titanium exhibit a somewhat erratic pattern; therefore, it is not surprising that the model does not match these values as closely. The model results for niobium are extremely close to the analytical values, largely due to the revision steps of the model. The calculated values for zirconium are also fairly good, even though only minor adjustments were made during the revision process.

As shown in Table 11, the model calculations for alkaline earth elements are extremely good in comparison with the analytical data. Both the calculation and the measurements for magnesium suggest that the solubility of this element is below any reliable analytical detection limit. The predictions for metal oxides are not as good. All but copper are within an order of magnitude, which is a reasonable expectation for a brief study such as this one. Even though the deviation for copper is about a factor of 20 from the

Table 11. Comparison of experimental and predicted inventories of impurity materials in average SRS simulant

Element	Solubility limit ($10 M^5$)		Solid species	
	Expt.	Calc.	Expt.	Calc.
Mg ²⁺	<2.3	<1		Mg(OH) ₂
Ca ²⁺	2.72	2.7		CaCO ₃
Sr ²⁺	3.06	1.1	SrCO ₃	SrCO ₃
Ba ²⁺	1.68	1.5	BaSO ₄	BaSO ₄
Cu(II)	349	18		Cu(OH) ₂
Fe(II)	15.7	2		Fe(OH) ₂
Fe(III)		3.2		Fe ₂ O ₃
Hg(II)	5.1	36		HgO
Ni(II)	<1.4			
Pb(II)	1.03E+04	5.05E+03		PbO
Zn(II)	4.69E+03	2.80E+04		Zn(OH) ₂

Note: Expt. = experimental; Calc. = calculated.

experimental value, it still gives a good indication of the qualitative behavior of this element. It should be noted that the model considered only one anion complex for each element—a restriction that may be a small source of error (would need to be demonstrated for this system). In addition, other solids may form instead of, or in addition to, the principal oxides and hydroxides that were considered. Finally, although the model considered only ion interactions between Na⁺ and each of the metal ion complexes, the effects of other anions may also be significant.

4. REFERENCES

1. Technical Task Request No. HLW-SDT-TTR-99-37.2, Westinghouse Savannah River Site, 12/20/99.
2. D. A. Bostick, R. D. Hunt, C. H. Mattus, W. V. Steele, and C. F. Weber, *Technical Task Plan for Waste and Simulant Precipitation Issues*, ORNL/CF-99/65 (Dec. 29, 1999).
3. G. Erikson, *Chem. Scripta* **8**, 100 (1975).
4. C. F. Weber, *J. Comp. Phys.* **145**, 655 (1998).
5. D. D. Walker, *Preparation of Simulant Waste Solutions*, WSRC-TR-99-00116 (Apr. 15, 1999).
6. K. S. Pitzer, *Activity Coefficients in Electrolyte Solution*, Second Edition, CRC Press, Boca Raton, Fla., 1991.

7. C. F. Weber, *A Solubility Model for Aqueous Solutions Containing Sodium, Fluoride, and Phosphate*, Ph.D. dissertation, The University of Tennessee, Knoxville, Tenn., 1998.
8. C. F. Baes and R. E. Mesmer, *The Hydrolysis of Cations*, Wiley, New York, 1976.
9. S. E. Ziemniak, M. E. Jones, and K. E. S. Combs, *J. Solution Chem.* **22**(7), 601–23 (1993).
10. HSC Chemistry for Windows, Version 2.0, Outokumpu Research, May 31, 1994.
11. M. V. Auger, *Compt. Rend.* **177**, 1302–4 (1923).
12. V. P. Vasil'ev, P. N. Vorob'ev, and I. L. Khodakovskii, *Russ. J. of Inorg. Chem.* **19**(10), 1481–3, (1974).
13. A. C. Fraker and A. W. Ruff, "The Effect of Solution pH on the Saline Water Corrosion of Titanium Alloys," *Titanium Science and Technology*, R. I. Jaffee and H. M. Burte, eds., Plenum Press, New York, 1973.
14. M. H. Bedford, *J. Amer. Chem. Soc.* **27**, 1216 (1905).
15. E. F. Smith and W. K. Van Haagen, *J. Amer. Chem. Soc.* **37**(8), 1783 (1915).
16. P. Sue, *Ann. Chim. (Ser. 11)* **7**, 33 (1937).
17. B. K. Sen, P. Bandyopadhyay, and A. V. Saha, *Mat. Res. Bull.* **17**, 611–20 (1982).
18. E. Shock, D. C. Sassani, M. Willis, and D. A. Sverjensky, *Geochim. Cosmochim. Acta* **61**, 907–51 (1997).
19. G. Jander and D. Ertel, *J. Inorg. Nucl. Chem.* **14**, 71–85 (1960).
20. N. Etxebarria, L. A. Fernandez, and J. M. Madariaga, *J. Chem. Soc. Dalton Trans.*, 3055 (1994).
21. B. Spinner, *Rev. Chim. Miner.* **5**, 839 (1968).
22. G. Neumann, *Acta Chem. Scand.* **18**, 278 (1964).
23. A. K. Babko, V. V. Lukachina, and B. I. Nabivanets, *Russ. J. Inorg. Chem.* **8**(8), 957–61 (1963).
24. A. V. Lapinsky, L. N. Shishkina, M. A. Pchelkina, and B. A. Stepanov, *J. General Chem of the USSR in English Trans.* **25**, 1805–9 (1955).
25. I. A. Sheka and Ts. V. Pevzner, *Russ. J. Inorg. Chem.* **5**(10), 1119–21 (1960).
26. H. Bilinski, M. Branica, and L. G. Sillen, *Acta Chem. Scand.* **20**, 853–61 (1966).
27. A. A. Slobodov, A. V. Kritskii, V. I. Zarembo, and L. V. Puchkov, *Zh. Prik. Khim.* **65**(5), 1031–1041 (1992).
28. S. U. Aja, S. A. Wood, and A. E. Williams-Jones, *Appl. Geochemistry* **10**, 603–20 (1995).
29. K. A. McGee and P. B. Hostetler, *J. Res. U.S. Geol. Survey*, **5**(2), 227–33 (1977).
30. V. A. Phillips, J. L. Kolbe, and H. Opperhauser, *J. Crystal Growth* **41**, 228–34 (1977).
31. C. F. Weber and E. C. Beahm, *Chemical Modeling of Waste Sludges*, ORNL/TM-13200 (1996).
32. L. B. Yeatts and W. L. Marshall, *J. Phys. Chem.* **71**(8), 2641–50 (1967).
33. L. N. Plummer and E. Busenberg, *Geochim. Cosmochim. Acta* **46**, 1011–40 (1982).
34. W. F. Linke, *Solubilities*, American Chemical Society, Washington, D.C., 1965.
35. E. Busenberg, L. N. Plummer, and V. B. Parker, *Geo. Cosmo. Acta* **48**, 2021–35 (1984).
36. E. Busenberg and L. N. Plummer, *Geo. Cosmo. Acta* **50**, 2225–33 (1986).
37. K. Ishikawa et al., *Hydrometallurgy* **45**, 129–35 (1997).
38. K. Zheng, R. St. C. Smart, J. Addai-Mensah, and A. Gerson, *J. Chem. Eng. Data* **43**, 312–317 (1998).

39. K. Zheng, J. Addai-Mensah, A. Gerson, and R. St. C. Smart, *J. Crystal Growth* **171**, 197–208 (1997).
40. M. C. Barnes, J. Addai-Mensah, and A. R. Gerson, *Collids Surfaces A: Physicochem. Eng. Aspects* **157**, 101–116 (1999).

Appendix A

Table A.1. Coefficients for Gibbs energy of formation

$$\Delta G^0/RT = A + B (T - T_0) + C (1/T_0 - 1/T) + D \ln(T/T_0) + E (T^2 - T_0^2)$$

	A	B	C	D	E	Ref.
Ar	0	0	0	0	0	
H ₂ O	-95.665	-1.0029	0	324.04	0.00050848	1
Na ⁺	-105.73	0.85194	0	0	-0.00088327	1
K ⁺	-114.043	0.881018	0	0	-0.00090498	1
H ⁺	0	0	0	0	0	
UO ₂ ²⁺	-384.948	3.675784	0	0	-0.0038481	1
NO ₃ ⁻	-43.984	0.68002	0	0	-0.00067471	1
OH ⁻	-63.534	0.75606	0	0	-0.00074688	1
Cl ⁻	-52.928	0.367999	0	0	-0.000358	1
F ⁻	-112.59	1.1322	0	0	-0.0011431	1
PO ₄ ³⁻	-411.192	4.33069	0	0	-0.00436232	1
HPO ₄ ²⁻	-439.592	4.74018	0	0	-0.0049977	3
NO ₂ ⁻	-32.066	0.081045	0	0	0.00027244	1
Al(OH) ₄ ⁻	-520.749	5.22566	0	0	-0.0053938	1
CO ₃ ²⁻	-213.14	2.28402	0	0	-0.0022976	1
HCO ₃ ⁻	-236.948	2.40768	0	0	-0.0024709	1
SO ₄ ²⁻	-300.531	3.11291	0	0	-0.00315535	1
Si(1,1)	-505.484	0	0	0	0	2
Si(2,1)	-474.791	0	0	0	0	2
Si(2,2)	-456.454	0	0	0	0	
Si(4,2)	-423.707	0	0	0	0	
Si(6,3)	-375.442	0	0	0	0	
Si(4,4)	-408.603	0	0	0	0	
Si(6,6)	-359.968	0	0	0	0	
Si(4,8)	-371.828	0	0	0	0	
Si(8,8)	-358.18	0	0	0	0	
C ₂ O ₄ ²⁻	-272.165	2.782581	0	0	-0.00279223	1
Si(0,1)	-528.074	0	0	0	0	2
Al(OH) ₃	459.665	4.51734	0	0	-0.0046758	6
NaNO ₃	-147.22	1.956587	0	-44.4701	-0.0019822	
KNO ₃	-158.891	0	0	0	0	
NaCl	-155.03	1.198614	0	0	-0.0012	
KCl	-164.878	0	0	0	0	4
NaF	-219.391	2.022907	0	0	-0.00208712	5
TSP	-1926.92	-1350.9963	-4E+07	415570.9	0.73117129	3
DSP	-1803.47	7.65392	0	0	0	3
DS	-3512.45	36.15256	0	0	-0.0377395	5
UO ₂ (OH) ₂	532.673	5.422982	0	0	-0.0056086	

Table A.1 (continued)

	A	B	C	D	E	Ref.
Na ₂ U ₂ O ₇	-1113.06	11.34351	0	0	-0.0117463	7
SiO ₂ (am)	-342.911	0	0	0	0	2
Nepheline	-798.771	0	0	0	0	
Kaolinite	-1532.77	0	0	0	0	
Cancrinite	-5454.57	0	0	0	0	
Soddyite	-1483.56	0	0	0	0	8
Na-boltw	-1395.59	0	0	0	0	8
Weeksite	-4817.96	0	0	0	0	8
Na ₂ C ₂ O ₄	-489.42	1.78964	0	0	-0.00188522	
Na ₂ SO ₄	-513.057	4.78648	0	0	-0.0049029	
Na ₂ SO ₄ *10H ₂ O	-1472.02	15.5281	0	0	-0.0162385	
Na ₂ SO ₄ *NaNO ₃ *2H ₂ O	-852.691	8.84139	0	0	-0.0093188	

References:

1. HSC Chemistry for Windows, Version 2.0, Outokumpu Research, May 31, 1994.
2. CODATA Key Values for Thermodynamics, J. D. Cox, D. D. Wagman, V. A. Medvedev, eds., Hemisphere Publishing Corp., 1986.
3. C. F. Weber et al., *J. Soln. Chem.* **28**(11), 1207 (1999).
4. C. F. Weber and E. C. Beahm, *Chemical Modeling of Waste Sludges*, ORNL/TM-13200 (1996).
5. C. F. Weber et al., *Ind. Eng. Chem. Res.* **39**, 518-26 (2000).
6. D. J. Wesolowski, *Geochem. Cosmochem. Acta* **56**, 1065 (1992)
7. D. T. Hobbs and D. G. Karraker, *Nucl. Technol.* **114**, 318-24 (1996); K. H. Gayer and H. Leider, *J. Am. Chem. Soc.* **77**, 1448-50 (1955).
8. Nguyen et al., *J. Chem. Thermodyn.* **24**, 359-76 (1992).

Table A.2. Pitzer parameters in basic model

Species		Parameter	Coefficients ^a				Ref. ^b
			A	B	C	D	
Na ⁺	K ⁺	θ	-0.012				1
Na ⁺	H ⁺	θ	0.036				1
Na ⁺	UO ₂ ²⁺	θ	-1.5027				
Na ⁺	NO ₃ ⁻	$\beta^{(0)}$	0.00204	0	406.5	-1.04	
Na ⁺	NO ₃ ⁻	$\beta^{(1)}$	0.2368	0	712.4	-1.214	
Na ⁺	NO ₃ ⁻	C	0.00008	0	-27.22	0.0756	
Na ⁺	OH ⁻	$\beta^{(0)}$	0.0864	0	531.5	-1.625	4
Na ⁺	OH ⁻	$\beta^{(1)}$	0.253	0	894.4	-2.7478	4
Na ⁺	OH ⁻	C	0.0021	0	-40.69	0.1158	4
Na ⁺	Cl ⁻	$\beta^{(0)}$	0.0759	0	280.3	-0.7339	4
Na ⁺	Cl ⁻	$\beta^{(1)}$	0.2765	0	-128.9	0.643	1
Na ⁺	Cl ⁻	C	0.00065	0	-14.7	0.03392	1
Na ⁺	F ⁻	$\beta^{(0)}$	0.033	0	246.8	-0.6728	6
Na ⁺	F ⁻	$\beta^{(1)}$	0.2456	0	2833	-9.451	6
Na ⁺	F ⁻	C	0.00281	0	12.25	-0.0436	6
Na ⁺	PO ₄ ³⁻	$\beta^{(0)}$	0.2534	0	130.3	0.1247	3
Na ⁺	PO ₄ ³⁻	$\beta^{(1)}$	3.7384	0	23420	-70.37	3
Na ⁺	PO ₄ ³⁻	C	-0.0226	0	0	-0.00016	3
Na ⁺	HPO ₄ ²⁻	$\beta^{(0)}$	-0.03045	0	1826	-5.159	3
Na ⁺	HPO ₄ ²⁻	$\beta^{(1)}$	1.3504	0	6023	-18.77	3
Na ⁺	HPO ₄ ²⁻	C	0.00359	0	-282.6	0.8267	3
Na ⁺	NO ₂ ⁻	$\beta^{(0)}$	0.05816	0	-4.606	0.11	
Na ⁺	NO ₂ ⁻	$\beta^{(1)}$	0.1363	0	4559	-12.98	
Na ⁺	NO ₂ ⁻	C	-0.0019	0	8.801	-0.0305	
Na ⁺	Al(OH) ₄ ⁻	$\beta^{(0)}$	0.0508	0	531.5	-1.625	7
Na ⁺	Al(OH) ₄ ⁻	$\beta^{(1)}$	0.253	0	894.4	-2.7478	7
Na ⁺	Al(OH) ₄ ⁻	C	-0.0005	0	-40.69	0.1158	7
Na ⁺	CO ₃ ²⁻	$\beta^{(0)}$	0.0362	-0.0233	-1108.38	11.19856	5
Na ⁺	CO ₃ ²⁻	$\beta^{(1)}$	1.51	-0.09989	-4412.51	44.58207	5
Na ⁺	CO ₃ ²⁻	C	0.00184				5
Na ⁺	HCO ₃ ⁻	$\beta^{(0)}$	0.028	-0.01446	-682.886	6.899586	5
Na ⁺	HCO ₃ ⁻	$\beta^{(1)}$	0.044	-0.02447	-1129.39	11.41086	5
Na ⁺	SO ₄ ²⁻	$\beta^{(0)}$	-0.01358	0	654	-1.691	1
Na ⁺	SO ₄ ²⁻	$\beta^{(1)}$	0.6998	0	1143	-2.164	1

Table A.2 (continued)

Species	Parameter	Coefficients ^a				Ref. ^b	
		A	B	C	D		
Na ⁺	SO ₄ ²⁻	C	0.00394	0	-37.95	0.0955	1
Na ⁺	Si(1,1)	β ⁽⁰⁾	0.0734				
Na ⁺	Si(1,1)	β ⁽¹⁾	2.7216				
Na ⁺	Si(1,1)	C	-0.0108				
Na ⁺	Si(2,1)	β ⁽⁰⁾	0.2182				
Na ⁺	Si(2,1)	β ⁽¹⁾	9.9072				
Na ⁺	Si(2,1)	C	-0.0074				
Na ⁺	Si(2,2)	β ⁽⁰⁾	-0.3282				
Na ⁺	Si(2,2)	β ⁽¹⁾	2.7191				
Na ⁺	Si(2,2)	C	0.0165				
Na ⁺	Si(4,2)	β ⁽⁰⁾	0.1927				
Na ⁺	Si(4,2)	β ⁽¹⁾	7.6205				
Na ⁺	Si(4,2)	C	-0.0063				
Na ⁺	Si(6,3)	β ⁽⁰⁾	-0.0441				
Na ⁺	Si(6,3)	β ⁽¹⁾	-0.4372				
Na ⁺	Si(6,3)	C	0.01				
Na ⁺	Si(4,4)	β ⁽⁰⁾	-0.1954				
Na ⁺	Si(4,4)	β ⁽¹⁾	1.4228				
Na ⁺	Si(4,4)	C	0.0105				
Na ⁺	Si(6,6)	β ⁽⁰⁾	-0.2761				
Na ⁺	Si(6,6)	β ⁽¹⁾	4.3188				
Na ⁺	Si(6,6)	C	0.0149				1
Na ⁺	Si(4,8)	β ⁽⁰⁾	-0.1265				
Na ⁺	Si(4,8)	β ⁽¹⁾	-0.5069				
Na ⁺	Si(4,8)	C	0.0087				
Na ⁺	Si(8,8)	β ⁽⁰⁾	-0.2457				
Na ⁺	Si(8,8)	β ⁽¹⁾	4.5521				
Na ⁺	Si(8,8)	C	0.0131				
Na ⁺	C ₂ O ₄ ²⁻	β ⁽⁰⁾	0.3249	0	17.36		
Na ⁺	C ₂ O ₄ ²⁻	β ⁽¹⁾	-0.0288	0	0.1478		
Na ⁺	C ₂ O ₄ ²⁻	C	-0.0483	0	4.58		
K ⁺	H ⁺	θ	0.005				1
K ⁺	NO ₃ ⁻	β ⁽⁰⁾	-0.0816				
K ⁺	NO ₃ ⁻	β ⁽¹⁾	0.0494				
K ⁺	NO ₃ ⁻	C	0.0033				
K ⁺	OH ⁻	β ⁽⁰⁾	0.1298				

Table A.2 (continued)

Species	Parameter	Coefficients ^a				Ref. ^b	
		A	B	C	D		
K ⁺	OH ⁻	$\beta^{(1)}$	0.32				
K ⁺	OH ⁻	C	0.002				
K ⁺	Cl ⁻	$\beta^{(0)}$	0.04787	0	217.7	-0.5586	1
K ⁺	Cl ⁻	$\beta^{(1)}$	0.2203	0	-274.8	1.2057	1
K ⁺	Cl ⁻	C	-0.00037	0	-11.95	0.03071	1
K ⁺	F ⁻	$\beta^{(0)}$	0.08089				1
K ⁺	F ⁻	$\beta^{(1)}$	0.2021				1
K ⁺	F ⁻	C	0.00046				1
K ⁺	PO ₄ ³⁻	$\beta^{(0)}$	0.2585				
K ⁺	PO ₄ ³⁻	$\beta^{(1)}$	4.316				
K ⁺	PO ₄ ³⁻	C	-0.00029				
K ⁺	HPO ₄ ²⁻	$\beta^{(1)}$	1.2743				1
K ⁺	HPO ₄ ²⁻	C	0.0058				1
K ⁺	NO ₂ ⁻	$\beta^{(0)}$	0.02073				
K ⁺	NO ₂ ⁻	$\beta^{(1)}$	-0.01379				
K ⁺	NO ₂ ⁻	C	-0.001				
K ⁺	Al(OH) ₄ ⁻	$\beta^{(0)}$					7
K ⁺	Al(OH) ₄ ⁻	$\beta^{(1)}$					7
K ⁺	Al(OH) ₄ ⁻	C					7
K ⁺	CO ₃ ²⁻	$\beta^{(0)}$	0.1288	0.0011	-1.81E-05	0	5
K ⁺	CO ₃ ²⁻	$\beta^{(1)}$	1.433	0.00436	-0.00119	0	5
K ⁺	CO ₃ ²⁻	C	-0.00018	0	0	0	5
K ⁺	HCO ₃ ⁻	$\beta^{(0)}$	-0.01071	0.001	0.000699	-4.70E-06	5
K ⁺	HCO ₃ ⁻	$\beta^{(1)}$	0.0478	0.0011	-0.00094	6.16E-06	5
H ⁺	NO ₃ ⁻	$\beta^{(0)}$	0.1168				1
H ⁺	NO ₃ ⁻	$\beta^{(1)}$	0.3546				1
H ⁺	NO ₃ ⁻	C	-0.0027				1
H ⁺	Cl ⁻	$\beta^{(0)}$	0.1769				1
H ⁺	Cl ⁻	$\beta^{(1)}$	0.2973				1
H ⁺	Cl ⁻	C	0.000362				1
UO ₂ ²⁺	NO ₃ ⁻	$\beta^{(0)}$	0.4607				
UO ₂ ²⁺	NO ₃ ⁻	$\beta^{(1)}$	1.6133				
UO ₂ ²⁺	NO ₃ ⁻	C	-0.01115				
UO ₂ ²⁺	OH ⁻	$\beta^{(0)}$	0.4274				

Table A.2 (continued)

Species		Parameter	Coefficients ^a				Ref. ^b
			A	B	C	D	
UO ₂ ²⁺	OH ⁻	β ⁽¹⁾	1.644				
UO ₂ ²⁺	OH ⁻	C	-0.01303				
UO ₂ ²⁺	Cl ⁻	β ⁽⁰⁾	0.4607				
UO ₂ ²⁺	Cl ⁻	β ⁽¹⁾	1.6133				
UO ₂ ²⁺	Cl ⁻	C	-0.01115				
UO ₂ ²⁺	CO ₃ ²⁻	β ⁽⁰⁾	0.4607				
UO ₂ ²⁺	CO ₃ ²⁻	β ⁽¹⁾	1.6133				
UO ₂ ²⁺	CO ₃ ²⁻	C	-0.01115				
UO ₂ ²⁺	HCO ₃ ⁻	β ⁽⁰⁾	0.322				
UO ₂ ²⁺	HCO ₃ ⁻	β ⁽¹⁾	1.827				
UO ₂ ²⁺	HCO ₃ ⁻	C	-0.0176				
NO ₃ ⁻	OH ⁻	θ	-0.0547				2
NO ₃ ⁻	Cl ⁻	θ	0.016				1
NO ₃ ⁻	Al(OH) ₄ ⁻	θ	0.014				7
NO ₃ ⁻	SO ₄ ²⁻	θ	0.0673				
NO ₃ ⁻	C ₂ O ₄ ²⁻	θ	-0.1017				
OH ⁻	PO ₄ ³⁻	θ	0.1				3
OH ⁻	CO ₃ ²⁻	θ	0.1				1
OH ⁻	SO ₄ ²⁻	θ	-0.013				1
Cl ⁻	F ⁻	θ	-0.01				6
Cl ⁻	PO ₄ ³⁻	θ	0.2559				
Cl ⁻	CO ₃ ²⁻	θ	-0.053				8
Cl ⁻	HCO ₃ ⁻	θ	0.036				8
Cl ⁻	SO ₄ ²⁻	θ	0.03				1
F ⁻	PO ₄ ³⁻	θ	0.55				6
PO ₄ ³⁻	NO ₂ ⁻	θ	0.1047				
CO ₃ ²⁻	HCO ₃ ⁻	θ	0.09				
CO ₃ ²⁻	SO ₄ ²⁻	θ	0.02				1
HCO ₃ ⁻	SO ₄ ²⁻	θ	0.01				1
Na ⁺	K ⁺	NO ₃ ⁻	ψ	-0.006			2
Na ⁺	K ⁺	OH ⁻	ψ	0.004			
Na ⁺	K ⁺	Cl ⁻	ψ	-0.0018			1
Na ⁺	K ⁺	CO ₃ ²⁻	ψ	0.003			1
Na ⁺	K ⁺	HCO ₃ ⁻	ψ	-0.003			1

Table A.2 (continued)

Species	Parameter	Coefficients ^a				Ref. ^b
		A	B	C	D	
Na ⁺	K ⁺	SO ₄ ²⁻	ψ	-0.01		1
Na ⁺	H ⁺	NO ₃ ⁻	ψ	-0.00274		2
Na ⁺	H ⁺	Cl ⁻	ψ	-0.004		1
Na ⁺	UO ₂ ²⁺	NO ₃ ⁻	ψ	0.3879		
Na ⁺	UO ₂ ²⁺	OH ⁻	ψ	-0.2556		
Na ⁺	NO ₃ ⁻	OH ⁻	ψ	0.0002		2
Na ⁺	NO ₃ ⁻	Cl ⁻	ψ	-0.006		
Na ⁺	NO ₃ ⁻	Al(OH) ₄ ⁻	ψ	-0.0048		
Na ⁺	NO ₃ ⁻	SO ₄ ²⁻	ψ	0.00335		
Na ⁺	NO ₃ ⁻	C ₂ O ₄ ²⁻	ψ	0.0802		
Na ⁺	OH ⁻	Cl ⁻	ψ	-0.0063		1
Na ⁺	OH ⁻	F ⁻	ψ	-0.035		6
Na ⁺	OH ⁻	PO ₄ ³⁻	ψ	0.03		3
Na ⁺	OH ⁻	CO ₃ ²⁻	ψ	-0.017		1
Na ⁺	OH ⁻	SO ₄ ²⁻	ψ	-0.009		1
Na ⁺	Cl ⁻	F ⁻	ψ	-0.00218		6
Na ⁺	Cl ⁻	PO ₄ ³⁻	ψ	0		
Na ⁺	Cl ⁻	CO ₃ ²⁻	ψ	0.0085		1
Na ⁺	Cl ⁻	SO ₄ ²⁻	ψ	0		1
Na ⁺	Cl ⁻	SO ₄ ²⁻	ψ	0		
Na ⁺	F ⁻	PO ₄ ³⁻	ψ	0		6
Na ⁺	F ⁻	HPO ₄ ²⁻	ψ	0		6
Na ⁺	PO ₄ ³⁻	NO ₂ ⁻	ψ	0.0537		
Na ⁺	CO ₃ ²⁻	HCO ₃ ⁻	ψ	0.002		1
Na ⁺	CO ₃ ²⁻	SO ₄ ²⁻	ψ	-0.005		1
Na ⁺	HCO ₃ ⁻	SO ₄ ²⁻	ψ	-0.005		1
K ⁺	H ⁺	NO ₃ ⁻	ψ	-0.0103		2
K ⁺	H ⁺	Cl ⁻	ψ	-0.011		2
K ⁺	NO ₃ ⁻	OH ⁻	ψ	-0.0032		2
K ⁺	NO ₃ ⁻	Cl ⁻	ψ	-0.0031		2
K ⁺	OH ⁻	Cl ⁻	ψ	-0.0032		2
K ⁺	OH ⁻	F ⁻	ψ	1.5956		
K ⁺	OH ⁻	CO ₃ ²⁻	ψ	-0.01		1
K ⁺	OH ⁻	SO ₄ ²⁻	ψ	-0.05		1

Table A.2 (continued)

Species	Parameter	Coefficients ^a				Ref. ^b
		A	B	C	D	
K ⁺ Cl ⁻ F ⁻	ψ	-0.0135				
K ⁺ Cl ⁻ CO ₃ ²⁻	ψ	0.004				1
K ⁺ Cl ⁻ HCO ₃ ⁻	ψ	-0.015				
K ⁺ Cl ⁻ SO ₄ ²⁻	ψ	-0.005				1
K ⁺ CO ₃ ²⁻ SO ₄ ²⁻	ψ	-0.009				1
K ⁺ HCO ₃ ⁻ SO ₄ ²⁻	ψ	0.005				

^aSee analagous equation for Gibbs energies in Table A.1.

^bNo reference indicates unpublished work of the authors.

References to Table A.2:

1. K. S. Pitzer, *Activity Coefficients in Electrolyte Solution*, 2nd Edition, CRC Press, Boca Raton, Fla., 1991.
2. C. F. Weber and E. C. Beahm, *Chemical Modeling of Waste Sludges*, ORNL/TM-13200 (1996).
3. C. F. Weber et al., *J. Soln. Chem.* **28**(11), 1207 (1999).
4. J. M. Simonson, *J. Chem. Thermodyn.* **21**, 561 (1989).
5. S. He and J. W. Morse, *Geochem. Cosmochem. Acta* **57**, 3533-54 (1993).
6. C. F. Weber et al., *Ind. Eng. Chem. Res.* **39**, 518-26 (2000).
7. D. J. Wesolowski, *Geochem. Cosmochem. Acta* **56**, 1065 (1992).
8. J. C. Peiper and K. S. Pitzer, *J. Chem. Thermodyn.* **14**, 613 (1982).

APPENDIX B

Table B.1. Filter 1—Solids present at point of NaNO₃ addition in average simulant

Filter name	Simulant	Filtration after component addition	Solid appearance	XRD analysis
WS02-F1	Average	NaNO ₃	Brown/tan	Al(OH) ₃ , NaNO ₃ >Na ₂ CO ₃ •H ₂ O>Na ₂ H(CO ₃) ₂ •H ₂ O

Composition of Simulant at point of precipitation

Temperature (°C) = 27.5

Simulant component	Amount Added (g)	Concentration of component (g/kg)	Molality
Water	674.18	---	---
NaOH	126.36	1.87E+02	4.69E+00
Al(NO ₃) ₃ •9H ₂ O	116.29	1.72E+02	4.60E-01
KNO ₃	1.5173	2.25E+00	2.23E-02
CsCl	0.0237	3.52E-02	2.09E-04
NaNO ₃	101.55	1.51E+02	1.77E+00

Table B.2. Filter 2—Solids present at point of NaF addition in average simulant

Filter name	Simulant	Filtration after component addition	Solid appearance	XRD analysis
WS02-F2	Average	NaF	Tan	$\text{Na}_2\text{CO}_3 \cdot \text{H}_2\text{O} > \text{Al}(\text{OH})_3 > \text{NaNO}_3$ + several minor peaks (1-2 phases)

Composition of simulant at point of precipitation

Temperature (°C) = 24.5

Simulant component	Amount added (g)	Concentration of component (g/kg)	Molality
Water	674.18	---	---
NaOH	126.36	1.76E+02	4.39E+00
$\text{Al}(\text{NO}_3)_3 \cdot 9\text{H}_2\text{O}$	116.29	1.62E+02	4.31E-01
KNO_3	1.5173	2.11E+00	2.09E-02
CsCl	0.0237	3.29E-02	1.96E-04
NaNO_3	101.55	1.41E+02	1.66E+00
NaNO_2	35.88	4.99E+01	7.23E-01
Na_2CO_3	16.96	2.36E+01	2.22E-01
Na_2SO_4	21.31	2.96E+01	2.08E-01
NaF	1.344	1.87E+00	4.45E-02

B-4

Table B.3. Filter 3—Solids present at point of Na₂C₂O₄ addition in average simulant

Filter name	Simulant	Filtration after component addition	Solid appearance	XRD analysis
WS02-F3	Average	Na ₂ C ₂ O ₄	White	Na ₂ C ₂ O ₄ >>Al(OH) ₃ +few minor peaks

Composition of simulant at point of precipitation Temperature (°C) = 31

Simulant component	Amount added (g)	Concentration of component (g/kg)	Molality
Water	674.18	---	---
NaOH	126.36	1.71E+02	4.27E+00
Al(NO ₃) ₃ •9H ₂ O	116.29	1.57E+02	4.19E-01
KNO ₃	1.5173	2.05E+00	2.03E-02
CsCl	0.0237	3.20E-02	1.90E-04
NaNO ₃	101.55	1.37E+02	1.62E+00
NaNO ₂	35.88	4.85E+01	7.03E-01
Na ₂ CO ₃	16.96	2.29E+01	2.16E-01
Na ₂ SO ₄	21.31	2.88E+01	2.03E-01
NaF	1.344	1.82E+00	4.33E-02
NaCl	1.461	1.98E+00	3.38E-02
Na ₂ C ₂ O ₄	1.072	1.45E+00	1.08E-02 *

*Assuming majority of Na₂C₂O₄ still in solution.

Table B.4. Filter 4—Solids present in final solution of average simulant

Filter name	Simulant	Filtration after component addition	Solid appearance	XRD analysis
WS02-F4	Average	Final	Tan	Na ₂ CO ₃ •H ₂ O>NaNO ₃ >10.1A phase (one peak)+few minor peaks

Composition of simulant at point of precipitation

Temperature (°C) = 30

Simulant component	Amount added (g)	Concentration of component (g/kg)	Molality
Water	674.18	---	---
NaOH	126.36	1.71E+02	4.27E+00
Al(NO ₃) ₃ •9H ₂ O	116.29	1.38E+02	3.69E-01
KNO ₃	1.5173	1.96E+00	1.93E-02
CsCl	0.0237	3.13E-02	1.86E-04
NaNO ₃	101.55	1.33E+02	1.57E+00
NaNO ₂	35.88	4.84E+01	7.02E-01
Na ₂ CO ₃	16.96	2.29E+01	2.16E-01
Na ₂ SO ₄	21.31	2.88E+01	2.03E-01
NaF	1.344	1.81E+00	4.31E-02
NaCl	1.461	1.97E+00	3.37E-02
Na ₂ C ₂ O ₄	1.072	1.45E+00	1.08E-02 *
Na ₂ HPO ₄ •12H ₂ O	3.585	3.36E+00	9.38E-03
Na ₂ SiO ₃ •9H ₂ O	1.137	1.54E+00	5.41E-03
Na ₂ MoO ₄ •2H ₂ O	0.048	6.49E-02	2.68E-04
Final water	327.9	---	---

*Assuming majority of Na₂C₂O₄ still in solution.

Table B.5. Filter 7—Solids collected after single filtration performed at completion of average simulant preparation

Filter name	Simulant	Filtration after component addition	Solid appearance	XRD analysis
WS02-F7	Average-total	Final	Brown amorphous, white crystals	$\text{Na}_2\text{C}_2\text{O}_4 > \text{NaNO}_3 > \text{Na}_2\text{CO}_3 \cdot \text{H}_2\text{O} > \text{Al}(\text{OH})_3$ + few minor peaks

Composition of simulant at point of precipitation

Temperature (°C) = 27.2

Simulant component	Amount added (g)	Concentration of component (g/kg)	Molality
Water	501.12	---	---
NaOH	126.36	1.01E+02	2.52E+00
$\text{Al}(\text{NO}_3)_3 \cdot 9\text{H}_2\text{O}$	116.30	9.29E+01	2.48E-01
KNO_3	1.5170	1.21E+00	1.20E-02
CsCl	0.0236	1.89E-02	1.12E-04
NaNO_3	101.56	8.12E+01	9.55E-01
NaNO_2	35.8816	2.87E+01	4.16E-01
Na_2CO_3	16.9639	1.36E+01	1.28E-01
Na_2SO_4	21.3109	1.70E+01	1.20E-01
NaF	1.3444	1.07E+00	2.56E-02
NaCl	1.4613	1.17E+00	2.00E-02
$\text{Na}_2\text{C}_2\text{O}_4$	1.072	8.57E-01	6.39E-03*
$\text{Na}_2\text{HPO}_4 \cdot 12\text{H}_2\text{O}$	3.5823	2.86E+00	7.99E-03
$\text{Na}_2\text{SiO}_3 \cdot 9\text{H}_2\text{O}$	1.135	9.07E-01	3.19E-03
$\text{Na}_2\text{MoO}_4 \cdot 2\text{H}_2\text{O}$	0.0482	3.85E-02	1.59E-04
Final water	To volume	---	---

*Assuming majority of $\text{Na}_2\text{C}_2\text{O}_4$ still in solution.

Table B.6. Filter 16—Solids collected after $\text{UO}_2(\text{NO}_3)_2$ added at completion of average simulant preparation

Filter name	Simulant	Filtration after component addition	Solid appearance	XRD analysis
WS02-16	Average-U end	Final	Orange-yellow amorphous; white amorphous & crystals	$\text{Na}_2\text{C}_2\text{O}_4 > \text{NaNO}_3 > \text{Na}_2\text{CO}_3 \cdot \text{H}_2\text{O}, (\text{UO}_2)\text{CO}_3 \cdot 2\text{H}_2\text{O}$, possible $\text{UO}_3 \cdot \text{H}_2\text{O}$ + few minor peaks

Composition of simulant at point of precipitation

Simulant component	Amount added (g)	Concentration of component (g/kg)	Molality
Water	499.90	---	---
NaOH	126.47	101.04	2.53E+00
$\text{Al}(\text{NO}_3)_3 \cdot 9\text{H}_2\text{O}$	116.31	92.92	2.48E-01
KNO_3	1.5176	1.21	1.20E-02
CsCl	0.02332	0.02	1.11E-04
NaNO_3	101.55	81.13	9.55E-01
NaNO_2	35.88	28.67	4.15E-01
Na_2CO_3	16.96	13.55	1.28E-01
Na_2SO_4	21.31	17.03	1.20E-01
NaF	1.3449	1.07	2.56E-02
NaCl	1.4614	1.17	2.00E-02
$\text{Na}_2\text{C}_2\text{O}_4$	1.0724	0.86	6.39E-03*
$\text{Na}_2\text{HPO}_4 \cdot 12\text{H}_2\text{O}$	3.582	2.86	7.99E-03
$\text{Na}_2\text{SiO}_3 \cdot 9\text{H}_2\text{O}$	1.137	0.91	3.20E-03
$\text{Na}_2\text{MoO}_4 \cdot 2\text{H}_2\text{O}$	0.0478	0.04	1.58E-04
$\text{UO}_2(\text{NO}_3)_2$	3.6780	0.01	0.00003**
Final water	To volume	---	---

* Assuming majority of $\text{Na}_2\text{C}_2\text{O}_4$ still in solution.

**Based on a soluble uranium concentration of 0.0004 M.

Table B.7. Filter 5—Solids present at point of NaNO₃ addition in high-NO₃⁻ simulant

Filter name	Simulant	Filtration after component addition	Solid appearance	XRD analysis
WS02-F5	High NO ₃ ⁻	NaNO ₃	White, amorphous	NaNO ₃ >Al(OH) ₃ >Al(NO ₃) ₃ •9H ₂ O+ Few minor peaks

Composition of simulant at point of precipitation

Temperature (°C) = 26

Simulant component	Amount added (g)	Concentration of component (g/kg)	Molality
Water	500	---	---
NaOH	98.4	1.97E+02	4.92E+00
Al(NO ₃) ₃ •9H ₂ O	120.04	2.40E+02	6.40E-01
KNO ₃	0.415	8.30E-01	8.21E-03
CsCl	0.0233	4.66E-02	2.77E-04
NaNO ₃	159.4	3.19E+02	3.75E+00

Table B.8. Filter 8—Solids present at point of NaF addition in high-NO₃⁻ simulant

Filter name	Simulant	Filtration after component addition	Solid appearance	XRD analysis
WS02-F8	High NO ₃ ⁻	NaF	Tan, amorphous, and ¼-in.-thick white solid	Na ₃ FSO ₄ >NaNO ₃ >unidentified phase(s)>Na ₂ CO ₃ •H ₂ O+ few minor peaks

Composition of simulant at point of precipitation

Temperature (°C) = 30.2

Simulant component	Amount added (g)	Concentration of component (g/kg)	Molality
Water	507.43	---	---
NaOH	98.41	100.24	2.51E+00
Al(NO ₃) ₃ •9H ₂ O	120.06	122.29	3.26E-01
KNO ₃	0.4155	0.4232	4.19E-03
CsCl	0.0236	0.0240	1.43E-04
NaNO ₃	159.43	162.39	1.91E+00
NaNO ₂	25.529	26.00	3.77E-01
Na ₂ CO ₃	16.960	17.28	1.63E-01
Na ₂ SO ₄	31.250	31.83	2.24E-01
NaF	2.1005	2.1395	5.10E-02

B-10

Table B.9. Filter 10—Solids present at point of Na₂C₂O₄ addition in high-NO₃⁻ simulant

Filter name	Simulant	Filtration after component addition	Solid appearance	XRD analysis
WS02-F10	High NO ₃ ⁻	Na ₂ C ₂ O ₄	White, amorphous, and white crystals	Na ₂ C ₂ O ₄ +few minor peaks

Composition of simulant at point of precipitation

Temperature (°C) = 30.2

Simulant component	Amount added (g)	Concentration of component (g/kg)	Molality
Water	507.43	---	---
NaOH	98.41	9.82E+01	2.45E+00
Al(NO ₃) ₃ •9H ₂ O	120.06	1.20E+02	3.19E-01
KNO ₃	0.4155	4.14E-01	4.10E-03
CsNCl	0.0236	2.35E-02	1.40E-04
NaNO ₃	159.43	1.59E+02	1.87E+00
NaNO ₂	25.5296	2.55E+01	3.69E-01
Na ₂ CO ₃	16.9604	1.69E+01	1.60E-01
Na ₂ SO ₄	31.2507	3.12E+01	2.19E-01
NaF	2.1005	2.10E+00	4.99E-02
NaCl	2.3383	2.33E+00	3.99E-02
Na ₂ C ₂ O ₄	1.0724	1.07E+00	7.98E-03*

*Assuming majority of Na₂C₂O₄ still in solution.

Table B.10. Filter 12—Solids present at point of Na₂SiO₃·9H₂O addition in high-NO₃⁻ simulant

Filter name	Simulant	Filtration after component addition	Solid appearance	XRD analysis
WS02-F12	High NO ₃ ⁻	Na ₂ SiO ₃ ·9H ₂ O	White, amorphous	NaNO ₃ >>Na ₃ HCO ₃ ·2H ₂ O>5.80A phase+few minor peaks

Composition of simulant at point of precipitation

Temperature (°C) = 29.2

Simulant Component	Amount added (g)	Concentration of component (g/kg)	Molality
Water	507.43	---	---
NaOH	98.41	9.62E+01	2.41E+00
Al(NO ₃) ₃ ·9H ₂ O	120.06	1.17E+02	3.13E-01
KNO ₃	0.4155	4.06E-01	4.02E-03
CsCl	0.0236	2.31E-02	1.37E-04
NaNO ₃	159.43	1.56E+02	1.83E+00
NaNO ₂	25.5296	2.50E+01	3.62E-01
Na ₂ CO ₃	16.9604	1.66E+01	1.57E-01
Na ₂ SO ₄	31.2507	3.06E+01	2.15E-01
NaF	2.1005	2.05E+00	4.89E-02
NaCl	2.3383	2.29E+00	3.91E-02
Na ₂ C ₂ O ₄	1.0724	1.05E+00	7.83E-03*
Na ₂ HPO ₄ ·12H ₂ O	3.5813	3.50E+00	9.78E-03
Na ₂ SiO ₃ ·9H ₂ O	1.1372	1.11E+00	3.91E-03

*Assuming majority of Na₂C₂O₄ still in solution.

Table B.11. Filter 6—Solids present at point of NaNO₃ addition in high-OH⁻ simulant

Filter name	Simulant	Filtration after component addition	Solid appearance	XRD analysis
WS02-F6	High OH ⁻	NaNO ₃	White & tan, amorphous	7.55A phase (very small crystallites) > Na ₂ CO ₃ •H ₂ O, Al(OH) ₃ , NaNO ₃ +few minor peaks

Composition of simulant at point of precipitation

Temperature (°C) = 27.4

Simulant component	Amount added (g)	Concentration of component (g/kg)	Molality
Water	545	---	---
NaOH	165.48	1.98E+02	4.95E+00
Al(NO ₃) ₃ •9H ₂ O	101.28	1.21E+02	3.23E-01
KNO ₃	3.0340	3.63E+00	3.59E-02
CsCl	0.0232	2.78E-02	1.65E-04
NaNO ₃	20.3698	2.44E+01	2.87E-01

Table B.12. Filter 11—Solids present at point of Na₂C₂O₄ addition in high-OH⁻ simulant

Filter name	Simulant	Filtration after component addition	Solid appearance	XRD analysis
WS02-F11	High OH ⁻	Na ₂ C ₂ O ₄	Slight tan film with white crystals	Na ₂ C ₂ O ₄ + few minor peaks

Composition of simulant at point of precipitation

Temperature (°C) = 26

Simulant component	Amount added (g)	Concentration of Component (g/kg)	Molality
Water	545	---	---
NaOH	165.48	1.77E+02	4.42E+00
Al(NO ₃) ₃ •9H ₂ O	101.28	1.08E+02	2.88E-01
KNO ₃	3.0340	3.24E+00	3.20E-02
CsCl	0.0232	2.48E-02	1.47E-04
NaNO ₃	20.3698	2.18E+01	2.56E-01
NaNO ₂	51.05	5.45E+01	7.90E-01
Na ₂ CO ₃	18.9222	2.02E+01	1.91E-01
Na ₂ SO ₄	4.27	4.56E+00	3.21E-02
NaF	0.4202	4.49E-01	1.07E-02
NaCl	0.5842	6.24E-01	1.07E-02
Na ₂ C ₂ O ₄	1.0724	1.15E+00	8.55E-03

*Assuming majority of Na₂C₂O₄ still in solution.

Table B.13. Filter 13—Solids present in final solution of high-OH⁻ simulant

Filter name	Simulant	Filtration after component addition	Solid appearance	XRD analysis
WS02-F13	High OH ⁻	Final	Slight tan amorphous film with white crystals	Na ₃ HCO ₃ -2H ₂ O>NaNO ₃ >Na ₂ CO ₃ •H ₂ O+few minor peaks

Composition of simulant at point of precipitation

Temperature (°C) = 25.5

Simulant component	Amount added (g)	Concentration of component (g/kg)	Molality
Water	545	---	---
NaOH	165.48	1.35E+02	3.36E+00
Al(NO ₃) ₃ -9H ₂ O	101.28	8.23E+01	2.20E-01
KNO ₃	3.0340	2.47E+00	2.44E-02
CsCl	0.0232	1.89E-02	1.12E-04
NaNO ₃	20.3698	1.66E+01	1.95E-01
NaNO ₂	51.05	4.15E+01	6.02E-01
Na ₂ CO ₃	18.9222	1.54E+01	1.45E-01
Na ₂ SO ₄	4.27	3.47E+00	2.44E-02
NaF	0.4202	3.42E-01	8.14E-03
NaCl	0.5842	4.75E-01	8.13E-03
Na ₂ C ₂ O ₄	1.0724	8.72E-01	6.51E-03
Na ₂ HPO ₄ •12H ₂ O	2.8665	2.33E+00	6.51E-03
Na ₂ SiO ₃ •9H ₂ O	1.371	1.11E+00	3.92E-03
Na ₂ MoO ₄ •2H ₂ O	0.0485	3.94E-02	1.63E-04
Final water	To volume	---	---

*Assuming majority of Na₂C₂O₄ still in solution.

INTERNAL DISTRIBUTION

- | | | | |
|-----|----------------|--------|-------------------------------|
| 1. | K. K. Anderson | 11. | S. M. Robinson |
| 2. | D. A. Bostick | 12. | B. B. Spencer |
| 3. | R. D. Hunt | 13–18. | W. V. Steele |
| 4. | R. T. Jubin | 19. | B. B. Spencer |
| 5. | T. E. Kent | 20. | H. Wang |
| 6. | D. D. Lee | 21–23. | C. F. Weber |
| 7. | A. J. Mattus | 24. | T. D. Welch |
| 8. | C. P. McGinnis | 25. | ORNL Central Research Library |
| 9. | L. E. McNeese | 26. | Laboratory Records, RC |
| 10. | K. E. Plummer | 27. | Laboratory Records, OSTI |

EXTERNAL DISTRIBUTION

28. Joe T. Carter, Westinghouse Savannah River Company, P.O. Box 616, 704-3N, Room S151, Aiken, SC 29808
29. Dennis Fennelly, UOP LLC, 307 Fellowship Road, Suite 207, Mt. Laurel, NJ 08054
30. Samuel D. Fink, Westinghouse Savannah River Company, P.O. Box 616, 773-A, Room B112, Aiken, SC 29808
31. Mark W. Geeting, Westinghouse Savannah River Company, P.O. Box 616, 704-196N, Room S411, Aiken, SC 29808
32. Roger L. Gilchrist, Pacific Northwest National Laboratory, P.O. Box 999, MS:K9-91, Richland, WA 99352
33. T. S. Gutmann, U.S. Department of Energy, Savannah River Operations Office, P.O. Box A, Aiken, SC 29802
34. H. D. Harmon, Tank Focus Area Salt Processing Program, P.O. Box 616, 704-3N, Room S151, Aiken, SC 29808
35. J. O. Honeyman, Lockheed Martin Hanford Corporation, P.O. Box 1500, MS: G3-21, Richland, WA 99352
36. R. A. Jacobs, Westinghouse Savannah River Company, P.O. Box 616, 704-3N, Room S252, Aiken, SC 29808
37. Jim Jewett, Numatec Hanford Corporation, P.O. Box 1970, Richland, WA 99352
38. Robert T. Jones, Westinghouse Savannah River Company, P.O. Box 616, 704-3N, Room S122, Aiken, SC 29808.
39. R. A. Kirkbride, Numatec Hanford Corporation, P.O. Box 1970, MS: H5-27, Richland, WA 99352
40. C. S. Louie, U.S. Department of Energy, Richland Operations Office, P.O. Box 550, MSIN: B4-55, Richland, WA 99352
41. James W. McCullough, U.S. Department of Energy, Savannah River Operations Office, P.O. Box A, Building 704-3N, Room S101, Aiken, SC 29802
42. J. P. Morin, Westinghouse Savannah River Company, P.O. Box 616, Savannah River Technology Center, 703-H, Aiken, SC 29808
43. Lynn Nelson, Westinghouse Savannah River Company, P.O. Box 616, 773-A, Room-B-112, Aiken, SC 29808

44. J. R. Noble-Dial, U.S. Department of Energy, Oak Ridge Operations Office, P.O. Box 2001, Oak Ridge, TN 37831-8620
45. Arlin Olson, Idaho National Engineering and Environmental Laboratory, Building 637, MS-5218, Idaho Falls, ID 83415-5218
46. L. M. Papouchado, Westinghouse Savannah River Company, P.O. Box 616, 773-A, Room A-263, Aiken, SC 29808
47. Reid Peterson, Westinghouse Savannah River Company, P.O. Box 616, 773-A, Room B-132, Aiken, SC 29808
48. S. F. Piccolo, Westinghouse Savannah River Company, P.O. Box 616, 704-3N, Room S152, Aiken, SC 29808
49. J. A. Pike, Westinghouse Savannah River Company, P.O. Box 616, 704-3N, Room S151, Aiken, SC 29808.
50. Michael Poirier, Westinghouse Savannah River Company, P.O. Box 616, 679-T, Room 2A6, Aiken, SC 29808
51. J. M. Reynolds II, U.S. Department of Energy, Savannah River Operations Office, P.O. Box A, Building 704-196N, Room S441, Aiken, SC 29802
52. Jim Rindfleisch, Idaho National Engineering and Environmental Laboratory, Building 637, MS-5218, Idaho Falls, ID 83415-5218
53. K. J. Rueter, Westinghouse Savannah River Company, P.O. Box 616, 706-S, Room 103, Aiken, SC 29808
54. S. N. Schlahta, Tank Focus Area Salt Processing Program, P.O. Box 616, 704-3N, Room S151, Aiken, SC 29808.
55. W. W. Schulz, 12704 Sandia Ridge Place NE, Albuquerque, NM 87111
56. Patricia C. Suggs, U.S. Department of Energy, Savannah River Operations Office, P.O. Box A, Building 704-196N, Room S431, Aiken, SC 29802
57. J. L. Swanson, 1318 Cottonwood, Richland, WA 99352
58. W. L. Tamosaitis, Westinghouse Savannah River Company, P.O. Box 616, 773-A, Room A-231, Aiken, SC 29808
59. Larry Tavlarides, Syracuse University, Dept. of Chemical Engineering & Materials Science, 334 Hinds Hall, Syracuse, NY 13244-1190
60. T. A. Todd, Idaho National Engineering and Environmental Laboratory, Building 637, MS-5218, Idaho Falls, ID 83415-5218
61. George Vandegrift, Argonne National Laboratory, Building 205, 9700 South Cass Avenue, Argonne, IL 60439
62. Darrel D. Walker, Westinghouse Savannah River Company, P.O. Box 616, 773-A, Room B-124, Aiken, SC 29808
63. Dennis W. Wester, Pacific Northwest National Laboratory, P.O. Box 999, MS: P7-25, 902 Battelle Boulevard., Richland, WA 99352
64. J. H. Westsik, Pacific Northwest National Laboratory, P.O. Box 999, MS:K9-91, Richland, WA 99352
65. W. R. Wilmarth, Westinghouse Savannah River Company, P.O. Box 616, 773-42A, Room 153, Aiken, SC 29808
66. P. E. Woodall, U.S. Department of Energy, Idaho Operations Office, 750 DOE Place (MS 1145), Idaho Falls, ID 83402
- 67-73. Tanks Focus Area Technical Team, c/o B. J. Williams, Pacific Northwest National Laboratory, P.O. Box 999, MSIN K9-69, Richland, WA 99352
74. Tanks Focus Area Field Lead, c/o T. P. Pietrok, U.S. Department of Energy, Richland Operations Office, P.O. Box 550, MS: K8-50, Richland, WA 99352